



Deposited via The University of Sheffield.

White Rose Research Online URL for this paper:

<https://eprints.whiterose.ac.uk/id/eprint/152441/>

Version: Accepted Version

---

**Article:**

Aschenbrenner, O., McGuire, P., Alsamaq, S. et al. (2011) Adsorption of carbon dioxide on hydrotalcite-like compounds of different compositions. *Chemical Engineering Research and Design*, 89 (9). pp. 1711-1721. ISSN: 0263-8762

<https://doi.org/10.1016/j.cherd.2010.09.019>

---

Article available under the terms of the CC-BY-NC-ND licence  
(<https://creativecommons.org/licenses/by-nc-nd/4.0/>).

**Reuse**

This article is distributed under the terms of the Creative Commons Attribution-NonCommercial-NoDerivs (CC BY-NC-ND) licence. This licence only allows you to download this work and share it with others as long as you credit the authors, but you can't change the article in any way or use it commercially. More information and the full terms of the licence here: <https://creativecommons.org/licenses/>

**Takedown**

If you consider content in White Rose Research Online to be in breach of UK law, please notify us by emailing [eprints@whiterose.ac.uk](mailto:eprints@whiterose.ac.uk) including the URL of the record and the reason for the withdrawal request.

# 1 Adsorption of carbon dioxide on hydrotalcite-like compounds 2 of different compositions

3  
4 Ortrud Aschenbrenner<sup>a</sup>, Paul McGuire<sup>b</sup>, Suzanne Alsamaq<sup>b</sup>, Jiawei Wang<sup>b</sup>,

5 Somsak Supasitmongkol<sup>a</sup>, Bushra Al-Duri<sup>b</sup>, Peter Styring<sup>a</sup> and Joseph Wood<sup>\*b</sup>

6 <sup>a</sup>Department of Chemical & Process Engineering, The University of Sheffield, Sir Robert Hadfield  
7 Building, Sheffield, UK, S1 3JD.

8 <sup>b</sup>School of Chemical Engineering, The University of Birmingham, Edgbaston, Birmingham, UK, B15  
9 2TT.

## 10 11 **Abstract**

12 The adsorption of carbon dioxide on hydrotalcite-like compounds was investigated. Two different  
13 powdered hydrotalcites were used containing the cations nickel and iron. The powdered materials  
14 were screened for carbon dioxide adsorption using a thermogravimetric method and it was found  
15 that NiMgAl (Sample 1) hydrotalcite has the largest capacity for CO<sub>2</sub>, adsorbing 1.58 mmol g<sup>-1</sup> at 20  
16 °C, and highest rate of adsorption of up to 0.17 mmol g<sup>-1</sup> min<sup>-1</sup>. This represented an increase of 53 %  
17 in adsorption capacity, compared with NiMgAlFe (Sample 2). In order to improve the rheological  
18 behaviour of hydrotalcite paste for extrusion, hydrotalcite powders were combined with boehmite  
19 alumina (70:30 and 50:50 ratios of hydrotalcite: boehmite) before extrusion into pellets suitable for  
20 use in a fixed bed adsorber. These pellets were then re-crushed and further tested by  
21 thermogravimetric methods. The effects of temperature, composition and pre-treatment of the  
22 hydrotalcites on the adsorption of carbon dioxide and nitrogen are reported. At 20 °C, the amount of  
23 carbon dioxide adsorbed was between 2.0-2.5 mmol g<sup>-1</sup> for all the hydrotalcite/alumina samples in  
24 this study, although this decayed rapidly with increasing temperature. The results are compared

1 with silica gel as a common sorbent reference, and with literature values. Hydrotalcite/alumina  
2 samples have thermal stability and a high adsorption capacity for carbon dioxide over a wide range of  
3 temperatures. The composition of the hydrotalcite/alumina pellets investigated in this study has less  
4 effect upon the adsorption behaviour compared with the non-calcined hydrotalcite powder, thus  
5 allowing a wide choice of pellet compositions to be used.

6  
7 Keywords: Adsorption, carbon dioxide, hydrotalcite, mixed oxide, carbon capture,  
8 thermogravimetric.

9

## 10 **1. Introduction**

11 In recent years, the need for reduction of carbon dioxide (CO<sub>2</sub>) emissions to prevent the  
12 anthropogenic contribution to climate change has become increasingly important (IPCC, 2007). One  
13 of the possible ways to achieve this is the capture of carbon dioxide from flue gas in industrial  
14 combustion processes and power plants. Various solid materials readily adsorb carbon dioxide. For  
15 example, calcium oxide or lithium oxide (Roesch et al., 2005; Mosqueda et al., 2006), silica gel (Wang  
16 and Levan, 2009; Huang et al., 2003), zeolites (Majchrzak-Kuceba and Nowak, 2005), activated  
17 carbon (Radosz et al., 2008) and hydrotalcites (Hutson and Attwood, 2008; Oliviera et al., 2008;  
18 Soares et al., 2005).

19 Hydrotalcites (Htlc) are a family of clay minerals consisting of a double-layered hydroxide  
20 structure, with the general formula  $[M^{II}_x M^{III}_{(1-x)}(OH)_2][CO_3]_{(1-x)/2} \cdot nH_2O$  (Cavani et al., 1991). They have  
21 a Brucite-like structure, whereby an M<sup>II</sup> or M<sup>III</sup> species is substituted almost isomorphously into the  
22 edge-sharing M(OH)<sub>6</sub> octahedra in place of Mg<sup>II</sup> to form sheets which have a net positive charge. The  
23 cationic sheets stack up on each other yielding a layered structure, with anions in the intercalating  
24 layers to balance the charge. Much previous work has concentrated on substituting various metals  
25 into the cationic layer (such as Ni<sup>2+</sup>, (Bhattacharyya et al., 1998; Olafsen et al., 2005; Perez-Lopez et  
26 al., 2006; Takehira et al., 2003; Tsyganok et al., 2003) Cu<sup>2+</sup>, Co<sup>2+</sup>, Fe<sup>2+</sup> (Unnikrishnan and Narayanan,

1 1999; Carja et al., 2001)  $\text{Cr}^{3+}$  (Kloprogge et al., 2005),  $\text{Fe}^{3+}$  (Ohisih et al., 2005) and  $\text{Mn}^{3+}$  (Barriga et  
2 al., 1996), whilst other work has concentrated on substituting various anions into the interstitial layer  
3 (Bhattacharyya and Hall, 1992; Tamura et al., 2004). Hydrotalcites adsorb carbon dioxide over a wide  
4 range of temperatures and can be used in pre-combustion (Walspurger et al., 2008) or post  
5 combustion capture (Soares et al., 2005) of carbon dioxide.

6 The composition (Hutson and Attwood, 2008) and preparation conditions (Kloprogge et al., 2005;  
7 Costantino et al., 1998) have been shown to influence the properties of hydrotalcites, such as surface  
8 area, and thus the amount of carbon dioxide they can adsorb. For example, addition of potassium as  
9 a promoter was found to increase the adsorption of carbon dioxide (Oliveira et al., 2008; Walspurger  
10 et al., 2008). The cation substituted into the Brucite layer has been shown to have a strong effect on  
11 physicochemical properties, such as surface area, pore structure and reducibility (Chmielarz et al.,  
12 2002). The anion also influences the structure of the finished hydrotalcite, particularly influencing  
13 the crystallinity and layer spacing (Tsyganok et al., 2003; Bhattacharyya and Hall, 1992; Carpani et al.,  
14 2004).

15 The main requirements for sorbents in carbon dioxide capture from flue gas are high capacity for  
16 carbon dioxide, high selectivity over nitrogen, low regeneration energy and high stability during  
17 subsequent sorption-desorption cycles. Various experimental data have been published on the  
18 adsorption of carbon dioxide on hydrotalcites. However, most of the adsorption studies in the  
19 literature were performed with hydrotalcites promoted with potassium or purely containing  
20 magnesium and aluminium cations. Few studies can be found about hydrotalcites with different  
21 compositions. Of those studies that have been published, Yong and Rodrigues (2002) reviewed  
22 progress on adsorption of carbon dioxide upon hydrotalcite like compounds. They found that the  
23 type of anion, cation and heat treatment influenced the adsorption capacity of carbon dioxide.  
24 Higher heat treatment, an optimal aluminium content and anions containing  $\text{CO}_3^{2-} / \text{Fe}(\text{CN})_6^{4-}$   
25 gave the best adsorption capacities. The optimum alumina content was a trade off between  
26 increased density of layer charge with increasing alumina, against decrease in the layer spacing as

1 alumina content increased. Anions leading to increased void space in the interlayer were found to  
2 lead to uptake of more carbon dioxide gas. Wang et al. (2008) studied the high temperature  
3 adsorption of carbon dioxide on mixed oxides derived from hydrotalcite like compounds. It was  
4 found that, for example, CaCoAlO captures  $1.39 \text{ mmol g}^{-1}$  of  $\text{CO}_2$  from a gas mixture (8 %  $\text{CO}_2$  in  $\text{N}_2$ ).  
5 Lwin and Abdullah (2009) studied the effect of Cu/Al ratio on the carbon dioxide capture  
6 characteristics of mixed oxides derived from hydrotalcites and found that for Cu/Al=1.0  
7 approximately  $30 \text{ mg g}^{-1}$  ( $0.68 \text{ mmol g}^{-1}$ ) carbon dioxide was adsorbed at a temperature of  $25 \text{ }^\circ\text{C}$ .  
8 Choi et al. (2009) reviewed the use of hydrotalcites, amongst other materials, for carbon dioxide  
9 capture and found that adsorption capacities at elevated temperatures ranged from  $0.17 - 0.9 \text{ mmol}$   
10  $\text{g}^{-1}$  at temperatures of  $473 - 773 \text{ K}$ . With renewed interest in carbon dioxide capture from stationary  
11 sources to comply with reductions in carbon capture emissions, new generations of adsorbents with  
12 increased carbon dioxide capture capacity are sought. Therefore there is new scope to further  
13 investigate and optimise the formulation of adsorbents such as hydrotalcites to understand what  
14 factors control their adsorption capacity and to increase it. In this study we present experimental  
15 results for the adsorption of carbon dioxide on hydrotalcites containing NiMgAl and iron (Fe) in  
16 different compositions. The effects of temperature and composition on stability, adsorption capacity  
17 and selectivity are discussed. The results are compared with silica gel as a cheap and available  
18 common sorbent.

19

## 20 **2. Experimental**

21

### 22 **2.1. Preparation of the samples**

23

#### 24 **2.1.1. Hydrotalcite preparation**

25

1 NiMgAl hydrotalcites were prepared by the co-precipitation of the relevant metal nitrates in a  
2 potassium carbonate solution. 1 M solutions of aluminium nitrate, magnesium nitrate and nickel  
3 nitrate were prepared separately then mixed in a ratio appropriate to yield hydrotalcites of the  
4 required composition after co-precipitation. The ratio fo Ni:Mg:Al ions of the synthesised  
5 hydrotalcite was 1:1:1. A sample was also prepared with a small amount of Fe<sup>3+</sup> ions in the ratio  
6 Ni:Mg:Al<sup>3+</sup>:Fe<sup>3+</sup> of 1:1:0.7:0.3. The 1 M mixed nitrate solution was diluted to 0.1 M with deionised  
7 water then added to the carbonate solution at a rate of 5 ml min<sup>-1</sup> at a temperature of 70 °C with  
8 vigorous stirring. A pH of 8.5 was maintained throughout the precipitation by the addition of 3 M  
9 sodium hydroxide from a peristaltic pump connected to a pH monitor and controller.

10 After the addition of the nitrate solution had ceased the hydrotalcite slurry was allowed to age,  
11 with the temperature and stirring maintained for a further 6 hours. The slurry was then filtered  
12 under vacuum and washed with five 800 ml of deionised water. The precipitate was dried in an oven  
13 in air at 65 °C for approximately 24 hours after which it was ground in an agate pestle and mortar  
14 and placed in an airtight container prior to further analysis.

15

### 16 **2.1.2. Mixed oxide preparation**

17

18 A 1g portion of the previously prepared hydrotalcite was calcined by heating in air to 600 °C at a rate  
19 of 10 °C min<sup>-1</sup> and holding at that temperature for 6 hours. A change in colour from light to dark  
20 green indicated the change from hydrotalcite to mixed oxide had occurred. The surface area and  
21 textural properties were then determined by N<sub>2</sub> adsorption experiments.

22

### 23 **2.1.3. Preparation of pellets for industrial application**

24

25 In order to utilise hydrotalcite for industrial carbon capture applications such as pressure or  
26 temperature swing adsorption, the powdered samples must be made into pellets suitable for use in a  
27 packed bed, since powdered samples would present too high a pressure drop under a flow of gas

1 through the bed. Methods for manufacturing pellets include pressing, tableting and extrusion,  
2 however the rheological properties of hydrotalcites are not favourable for extrusion unless the  
3 powder is mixed with other binders and flow aids to improve the properties of the paste, and  
4 therefore hydrotalcites were mixed with alumina prior to manufacturing the pellets. Four different  
5 hydrotalcite/alumina samples were studied, each with a different composition. For example, to  
6 make a 50 % hydrotalcite: 50 % alumina pellet, 25 g hydrotalcite samples were dry mixed with 25 g  
7 boehmite (aluminium oxide hydroxide) powder before adding 50 ml distilled water and kneading to  
8 make a paste with improved flow characteristics compared with hydrotalcite powder only. 2 g Acetic  
9 acid diluted in 10 ml of deionised water was then added in order to improve the paste rheology and  
10 impart some rigidity to the paste immediately after it has been extruded. The paste was extruded,  
11 cut into pellets of 2.5 mm diameter and 5 mm length, which were then further calcined by heating in  
12 air to 600 °C at a rate of 10 °C min<sup>-1</sup> for 6 hours. After calcination, the boehmite was converted to  
13 alumina. Pellets containing different ratios of hydrotalcite : boehmite (50:50 and 70:30) were  
14 manufactured from the powdered Sample 1 and Sample 2 samples. The compositions of the  
15 hydrotalcites are given in Table 1. Some pellets were retained for future studies in a fixed bed, whilst  
16 for the purposes of thermogravimetric tests the pellets were crushed to a fine powder. For the  
17 purposes of comparison of adsorption capacities, silica gel (for flash chromatography, particle size  
18 40-63 µm, BDH 153325P) was used as received.

19

## 20 **2.2. Characterisation of samples**

21

### 22 **2.2.1. Nitrogen adsorption**

23

24 The surface areas of the powdered mixed oxides and hydrotalcite/alumina pellets were determined  
25 by N<sub>2</sub> adsorption at liquid N<sub>2</sub> temperature using a Micromeritics ASAP 2020. The samples were first

1 outgassed under vacuum at 300 °C for a period of 12 hours. The average pore size was estimated  
2 from the isotherm using the BJH method on the desorption step.

3 Temperature programmed reduction (TPR) experiments were carried out on a Micromeritics  
4 Autochem II (2920). Approximately 50 mg of sample was used in all experiments. The samples were  
5 first held in a 10% H<sub>2</sub>/Ar mixture flowing at 100 cm<sup>3</sup> min<sup>-1</sup> at 100 °C for 1 hour. The temperature was  
6 then increased to 1000°C at a rate of 10 °C min<sup>-1</sup> (the TPR conditions thus meeting the Malet and  
7 Caballero (1988) conditions for TPR experiments) and the hydrogen consumption recorded.

8 Powder X-Ray Diffraction (XRD) was carried out on the fresh hydrotalcite and mixed oxides with a  
9 Siemens D5005 diffractometer in reflection mode using CuK $\alpha$  radiation. The Ni<sup>0</sup> crystallite sizes after  
10 reduction were estimated using the Scherrer equation from the (1 1 1) reflection.

11

### 12 **2.2.2. Thermogravimetric analysis experimental procedure**

13

14 A thermogravimetric analyser (Pyris 1 TGA, PerkinElmer) was used to investigate the stability,  
15 adsorption and desorption behaviour of the hydrotalcite/alumina samples. All experiments were  
16 performed at atmospheric pressure. Dry carbon dioxide (99.8%, BOC) and nitrogen (BOC) were used  
17 as purge gas at a constant flow of circa 50 cm<sup>3</sup> min<sup>-1</sup>.

18 The tests were carried out for the powdered hydrotalcite samples, powdered mixed oxide,  
19 powdered boehmite, and crushed hydrotalcite/alumina pellets. A sample of 5 to 15 mg was placed  
20 in a ceramic sample pan and suspended in the furnace of the thermogravimetric analyser. A fresh  
21 sample was used for each experiment. The furnace temperature was set in the range of 20 to 600 °C  
22 according to the experimental method as described below. The temperature of the sample was  
23 measured directly under the sample pan with a thermocouple.

24 The following method was used to investigate the stability of the hydrotalcite/alumina at high  
25 temperatures using the thermogravimetric analyser. The samples were held at 30 °C for 2 min and  
26 then heated to 600 °C at 10 °C min<sup>-1</sup>. In some experiments, subsequent cooling and re-heating cycles  
27 followed. As the cooling took much longer than the heating, a cooling rate of 50 °C min<sup>-1</sup> was used

1 and the furnace temperature was held at 30 °C for 20 min before the next heating cycle to 600 °C at  
2 10 °C min<sup>-1</sup> was started.

3 The adsorption and desorption experiments were performed in the thermogravimetric analyser  
4 using the following methods. The samples were degassed and dried directly prior to the  
5 experiments. For non-calcined hydrotalcite powders the sample powder was placed in the  
6 instrument and heated to 120 °C under carbon dioxide and held for 30 minutes. It was then cooled  
7 to just above ambient temperature (25 or 20 °C) and held for 90 minutes in a flow of carbon dioxide,  
8 until the weight remained constant. Finally the sample was heated to 140 °C for 8 minutes to desorb  
9 to the initial state. The above steps were repeated to check the regeneration capability of the  
10 sample. For the mixed oxide samples, which had already been calcined, a higher temperature for the  
11 initial heating procedure of 600 °C was used, before cooling to the adsorption temperature of 25 °C.

12

### 13 **3. Results and Discussion**

14

#### 15 **3.1. Sample characterisation**

16

##### 17 **3.1.1. Bet surface areas of samples**

18

19 Two powdered hydrotalcite samples were prepared by a precipitation method (Sample 1 and Sample  
20 2), and were subsequently converted into pellets suitable for use in an adsorber bed by mixing with  
21 boehmite to make a paste, extruding, drying and calcining (Samples 3-6). Boehmite is added to  
22 improve the rheological properties of the paste, resulting in the final pellet consisting of mixed  
23 hydrotalcite/alumina. Table 1 displays the compositions of each material, together with their BET  
24 surface areas determined by nitrogen sorption. Also shown for the purposes of comparison are the  
25 surface areas for boehmite powder. An isotherm obtained during the nitrogen sorption analysis is  
26 given in Fig. 1 for the mixed oxide. In all cases the adsorption/desorption experiments yielded an

1 isotherm closest in shape to the IUPAC type IV (Sing et al., 1985), displaying a marked hysteresis  
2 between the adsorption and desorption curves.

3 Isotherms of this type are characteristic of mesoporous materials, whereby the adsorption at  
4 lower values of  $P/P_0$  is consistent with the single layer/multi layer adsorption, also found with non-  
5 porous materials, whilst the distinct hysteresis at higher values of  $P/P_0$  indicates capillary  
6 condensation in the mesopores. The hysteresis is closest in shape to the H3 type (Sing et al., 1985).  
7 This type of hysteresis is reported to be consistent with 'slit-shaped' pores formed by aggregates of  
8 plate-like particles (Carrado et al., 2002). It is reasonable to expect that a mixed oxide derived from a  
9 hydrotalcite would display an isotherm and hysteresis of this type given the layered structure of the  
10 hydrotalcite from which it is derived.

11 The surface areas for the hydrotalcite powders show that the NiMgAl hydrotalcite (Sample 1) has  
12 a higher surface area than the iron containing Sample 2. These two samples were compared since  
13 there are suggestions in the literature that adding iron to the catalyst may improve its performance  
14 in the methane dry reforming reaction (Courson et al., 2000). Possibly, during heating to 300 °C for  
15 evacuation in the BET measurement, some of the hydrotalcite structure could have been destroyed  
16 and the mixed oxide formed. The surface areas and pore sizes obtained for the hydrotalcites are  
17 interesting when compared to other published data. For similar compositions they are in broad  
18 agreement with other published work, which report surface areas of between 150-200  $\text{m}^2\text{g}^{-1}$  (Perez-  
19 Lopez et al., 2006) or exceptionally as high as 300  $\text{m}^2\text{g}^{-1}$  when ultrasound is used during synthesis  
20 (Climent et al., 2004). Boehmite has a significantly higher surface area than hydrotalcite. After  
21 mixing with Boehmite, forming into pellets and calcining (Samples 3-6), the surface areas all lie within  
22 the range 200 – 234  $\text{m}^2\text{g}^{-1}$ , the 50 % hydrotalcite:50 % boehmite samples having the larger surface  
23 areas than the 70 % hydrotalcite:30 % boehmite materials. This suggests that the structures of the  
24 boehmite and hydrotalcite particles are maintained, such that the final surface area of the  
25 hydrotalcite/alumina is an average of the values recorded for each of the separate starting materials.  
26 Of the hydrotalcite powders prepared the NiMgAl (Sample 1) had the highest surface area, and

1 therefore was selected for further characterization as the most promising sample as a candidate  
2 adsorbent for carbon dioxide.

### 3 4 **3.1.2. Structure of NiMgAl hydrotalcite**

5  
6 An XRD pattern obtained for the synthesised NiMgAl hydrotalcite (Sample 1) powder is given in Fig.  
7 2. This pattern is consistent with ones previously published such as those by Clause et al. (1993), and  
8 is indicative of a material with a layered structure. Three relatively narrow peaks occur at low  $2\theta$   
9 values ( $2\theta = 11.6, 23.2, 34.8^\circ$ ) corresponding to the 003, 006 and 012 reflections (Cavani et al.,  
10 1991). The cell parameters can be estimated from these peaks and are calculated to be  $a = 3.04 \text{ \AA}$   
11 and  $c = 23.30 \text{ \AA}$  and the basal spacing  $d = 7.77 \text{ \AA}$ .

12 The composition of this hydrotalcite was examined by EDX in order to compare the nominal and  
13 actual composition of the synthesised materials. The measured  $M^{II}/M^{III}$  ratio was 2, in agreement  
14 with the expected value, and the measured Ni/Mg ratio was 0.98, with expected value 1.0, also  
15 displaying good agreement, suggesting that preferential precipitation of one of the metallic  
16 constituents did not occur.

17 After synthesis and analysis to confirm that the prepared materials were as expected, the  
18 hydrotalcites were calcined in air at  $600^\circ\text{C}$  for 6 hours. This step completely destroys the layered  
19 structure of the hydrotalcite resulting in a high surface area mixed oxide. As with the fresh  
20 hydrotalcite no dependence of structure on composition was found, a typical mixed oxide XRD trace  
21 obtained is given in Fig. 3.

22 It can be seen from Fig. 3 that the XRD pattern in Fig. 2 has been replaced by three diffuse peaks  
23 which indicate the presence of largely amorphous NiO, MgO and solid solutions of NiO/MgO. There  
24 are no peaks present relating to any aluminium oxide species such as spinel ( $\text{MgAl}_2\text{O}_4$ ), as they do not  
25 crystallise at the relatively low temperature at which the calcination was carried out.

26

### 3.1.3. Reduction behavior of NiMgAl hydrotalcite

The reduction properties of the mixed oxide of the Sample 1 were determined by TPR, and the results are shown in Fig. 4. The TPR trace displays three peaks, corresponding to NiO in various states of interaction with MgO. The short broad peak occurring at the lowest temperature is associated with the reduction of segregated NiO which occurs close to these temperatures (Perez-Lopez et al., 2006; Montoya et al., 2000; Parmaliana et al., 1990). Segregated NiO has previously been observed in nickel deficient hydrotalcite derived mixed oxides, the effect of the reduction peak moving towards higher temperatures with decreasing nickel content has also been previously observed (Perez-Lopez et al., 2006; Tichit et al., 1997). A 'shoulder' peak can be observed at approximately 550 °C, this peak is likely to correspond to NiO occupying surface sites in the MgO lattice, and although not directly commented on in previous work on hydrotalcites such as that by Perez-Lopez et al. (2006), it is seen in some of their TPR traces and observed in the TPR traces of non- hydrotalcite derived Ni/Al<sub>2</sub>O<sub>3</sub> catalysts prepared by the incipient wetness technique or by co-precipitation (Li and Chen, 1995). The peak occurring at the highest temperature (775 °C) corresponds to NiO interacting strongly with the MgO lattice ('bulk' NiO), this peak is a common feature of NiO/MgO solid solutions and mixed oxides.

### 3.2. Thermogravimetric analysis of hydrotalcite powders

Powdered hydrotalcite Samples 1 and 2 were analysed for carbon dioxide adsorption both before and after calcination, using a thermogravimetric method. Fig. 5 shows the CO<sub>2</sub> adsorption capacity of various hydrotalcite samples and boehmite during the first, second and third temperature cycle of heating from 30 °C to 600 °C, followed by cooling. The NiMgAl hydrotalcite (Sample 1) was observed to display the highest capacity of around 1.58 mmol CO<sub>2</sub> (g adsorbent)<sup>-1</sup>. This is significantly higher than the adsorption capacity of NiMgAlFe hydrotalcite (Sample 2), which only adsorbs around 1.03 mmol CO<sub>2</sub> (g adsorbent)<sup>-1</sup>. There are two possible reasons for the change in adsorption capacity. Firstly, the dispersion of nickel particles, which act as adsorption sites for carbon dioxide may be

1 influenced by the change of composition. Secondly, the pore size and surface area may be affected  
2 by the addition of iron, thus influencing the accessibility of carbon dioxide in to the pore structure.  
3 The Brucite-layered structure of hydrotalcites contains sheets of metal and hydroxide ions  
4 intercalated with anions and water molecules. Iron ( $\text{Fe}^{2+}$ ) has a relatively large ion radius of 0.76 Å,  
5 which is larger than the ion radii of  $\text{Mg}^{2+}$  and  $\text{Al}^{3+}$  ions of 0.65 and 0.6 Å respectively (Yu et al, 2008),  
6 and therefore  $\text{Fe}^{2+}$  may be difficult to be incorporated in to the hydrotalcite lattice. Another factor is  
7 the possible formation of a spinel phase ( $\text{NiFe}_2\text{O}_4$  or  $\text{FeFe}_2\text{O}_4$ ), which is more likely with increasing  
8 iron content. Sample 1 which does not contain iron, displays a surface area 19.3 % higher than  
9 Sample 2, which has iron incorporated in its structure (Table 1), which could be due to the difficulty  
10 of incorporating iron in to the lattice as mentioned above. Similarly Yu et al (2008) observed  
11 decreases in surface area with the increase in Fe content, which they attributed to the increased  
12 fraction of the spinel phase.

13 The effect of calcining the sample to produce the oxide form resulted in a reduced adsorption  
14 capacity of Sample 1, but an increase in the capacity of the Sample 2. The calcination to the oxide  
15 form would be expected to destroy the Brucite-layered structure. The collapse of the structure may  
16 lead to possible loss of surface area and adsorption capacity. Tichit et al (1997) noted that a three  
17 phase model is generally proposed for calcined LDH materials, which may comprise: Al-doped NiO or  
18 MgO crystallites, Ni- or Mg-doped alumina and an aluminate spinel-type phase at the Mg(Ni)O-  
19 alumina interface. The calcination could induce the formation of both the aluminate spinel-type  
20 phase and the Mg and/or Ni-doped alumina, with the spinel phase possibly leading to less adsorption  
21 capacity than the hydrotalcite as observed for Sample 1. However, the removal of water and carbon  
22 dioxide during calcination can lead to the formation of channels and pores, which could increase the  
23 specific surface area (Yu et al., 2008), and thus increase carbon dioxide adsorption as observed for  
24 Sample 2. The adsorption capacity of boehmite of  $1.3 \text{ mmol CO}_2 (\text{g adsorbent})^{-1}$  was in a similar  
25 range as that of the hydrotalcite samples. A strong influence of the hydrotalcite composition on the  
26 adsorption capacity was reported by Hutson and Attwood (2008) who found adsorption capacities  
27 for carbon dioxide in the range of 0.4 to  $3.6 \text{ mmol g}^{-1}$  at 330 °C for a variety of hydrotalcites with

1 different composition. In comparison with literature values, it also has to be considered that the  
2 adsorption capacity can depend on the calcination temperature (Hutson et al., 2004). Upon  
3 repeating the temperature cycles, the amount of CO<sub>2</sub> adsorbed at each cycle fell by a small amount,  
4 for example the amount of CO<sub>2</sub> adsorbed over Sample 1 hydrotalcite in the third cycle was 17 %  
5 lower than the first cycle. This reduction could possibly be due to sintering of the hydrotalcite  
6 particles at high temperature, leading to loss of surface area with increasing number of adsorption-  
7 desorption cycles. Fig. 6 shows the rate of adsorption of CO<sub>2</sub> over each sample, which indicates that  
8 Sample 1 displays the fastest adsorption rate of 0.17 mmol g<sup>-1</sup> min<sup>-1</sup>. The rate of adsorption of CO<sub>2</sub>  
9 upon Sample 1 during the first cycle is markedly faster than any of the other samples, but decreases  
10 with increasing number of cycles such that at the third cycle, the rate has fallen by 44 %.

11

### 12 **3.3. Thermal stability of hydrotalcite/alumina pellets**

13

14 Hydrotalcite powders were manufactured into pellets by mixing with boehmite in ratios of 50:50 or  
15 70:30 hydrotalcite:boehmite, before making into paste, extruding, drying and calcining. Since  
16 alumina derived from boehmite can also adsorb carbon dioxide, further detailed thermogravimetric  
17 studies were carried out on the hydrotalcite/alumina composite samples. Samples of crushed and  
18 ground hydrotalcite/alumina were heated to 600 °C (calcination temperature) at 10 °C min<sup>-1</sup> both  
19 under a nitrogen and carbon dioxide atmosphere. Fig. 7 shows the resulting weight loss curves for  
20 Sample 3. They are almost identical for nitrogen and carbon dioxide atmospheres. A weight loss of  
21 approximately 10% was observed on heating from 50 to 600 °C. The weight loss was constant and  
22 smooth. This indicates there was no decomposition but rather the loss of loosely bound molecules,  
23 which can be attributed to interlayer and surface water (Hutson et al., 2004). Usually,  
24 thermogravimetric curves of hydrotalcite samples show one or two further weight loss peaks at 250-  
25 600 °C, arising from dehydroxylation and decarbonisation respectively (Hutson et al., 2004; Othman  
26 et al., 2006). These decomposition processes occur during calcination and change the structure and  
27 surface of the hydrotalcites (Perez-Lopez et al., 2006). As the samples used in this study had already

1 undergone calcination prior to the experiments, no such decomposition processes were observed  
2 here. This indicates that re-heating of calcined samples does not result in further modification of the  
3 hydrotalcite structure. All four hydrotalcites showed virtually the same behaviour on heating to 600  
4 °C, as shown in Fig. 8. Thus, the composition of the hydrotalcite has no influence on the stability of  
5 the hydrotalcite structure at high temperatures. This was only thought to be valid for calcined  
6 samples, as hydrotalcites with different composition of the cations magnesium, cobalt and calcium  
7 were found to have different dehydroxylation and decarbonisation temperatures by Wang et al.  
8 (2008).

9 Experiments with silica gel as a standard adsorbent were performed for comparison. The sample  
10 was heated to 600 °C in carbon dioxide at 10°C min<sup>-1</sup>. The result is shown in Fig. 9 and was different  
11 from the behaviour of the hydrotalcites. A step was observed in the weight curve, indicating two  
12 different stages of weight loss. Initially the evaporation of water and desorption of gas occurs in a  
13 similar manner to the hydrotalcites. At approximately 300 °C, however, a second weight loss process  
14 takes place as the slope of the weight loss curve becomes steeper again. This indicates a  
15 decomposition process in the silica gel. Similar behaviour is obtained with nitrogen as the purge gas  
16 (not shown). Thus, hydrotalcites offer increased thermal stability compared to materials such as  
17 silica gel.

18 Subsequent cooling and re-heating cycles were performed. The results are shown in Fig. 10 for  
19 Sample 3. During the cooling process following the first heating, the mass remains nearly constant  
20 until temperatures lower than 300 °C are reached. This behaviour differs strongly from the heating  
21 process. Below 100 °C a steep increase in mass is observed during cooling, which is probably due to  
22 adsorption of the gas on the hydrotalcite. Re-heating results in a slow loss of mass. The amount of  
23 weight lost during this re-heating cycle at 600 °C equals the amount of weight increase during the  
24 previous cooling cycle, indicating that any adsorbed gas is completely desorbed at 600 °C. Hysteresis  
25 is observed for the cooling and heating of the hydrotalcite which might indicate that the desorption  
26 process is slower than the adsorption process. However, it is also possible that the hysteresis effect  
27 is caused by a slight temperature difference between the thermocouple, which was placed directly

1 under the sample holder, and the sample itself, during heating and cooling. The response of the  
2 actual hydrotalcite sample temperature may be slower than that of the thermocouple, thus causing  
3 the different behaviour for heating and cooling. This possible error can be excluded in the isothermal  
4 experiments described in the following sections.

5 After the initial loss of water in the first heating cycle, the cooling and heating cycles are  
6 reproducible, showing again that no structural damage or decomposition occurs. The behaviour of  
7 the hydrotalcite is virtually identical for carbon dioxide and for nitrogen atmosphere (not shown), so  
8 that the hysteresis seems to be a thermal effect, independent of the gas. However, the amount of  
9 weight increase/decrease during the hysteresis is slightly higher for carbon dioxide than for nitrogen.  
10 This may be an indication for higher adsorption of carbon dioxide on hydrotalcites compared to  
11 nitrogen.

12

### 13 **3.4. Effect of pre-treatment on carbon dioxide adsorption upon hydrotalcite/alumina pellets**

14

15 Sample 3 was pre-treated at different temperatures before carbon dioxide adsorption. In all cases,  
16 the sample had been calcined at 600 °C. The pre-treatment at elevated temperature mainly ensured  
17 there was no water adsorbed on the sample. Three different pre-treatment temperatures were used:  
18 150, 300 and 600 °C. The hydrotalcite was heated to the pre-treatment temperature for 60 min in  
19 case of 150 and 300 °C, and for 10 min in case of 600 °C, and then cooled to 20 °C for carbon dioxide  
20 adsorption. When adsorption equilibrium was reached, the hydrotalcite was re-heated for  
21 desorption.

22 The amount of carbon dioxide adsorbed increased with increasing pre-treatment temperature  
23 (Table 2). This is in agreement with the stability experiments which showed a high weight loss in the  
24 initial heating cycle. Obviously, any loosely bound molecules on the hydrotalcite occupy adsorption  
25 sites and hinder the adsorption of carbon dioxide. The best adsorption results were obtained with  
26 pre-treatment at 600 °C, the calcination temperature, for 10 min. Therefore this pre-treatment  
27 method was used for all further experiments.

1 Experiments were also performed for silica gel with different pre-treatment temperatures. Unlike  
2 the hydrotalcites, silica gel showed poorer adsorption performance upon pre-treatment at higher  
3 temperatures (Table 2). Pre-treatment at 600 °C for 10 min led to a lower adsorption of carbon  
4 dioxide at 20 °C than pre-treatment at 150 °C for 60 min. This is in line with the stability results  
5 which show some decomposition or change in structure at circa 300 °C. Therefore, the pre-treatment  
6 method at the lower temperature of 150 °C was used for silica gel in the low-temperature sorption  
7 experiments at 20 °C. For the experiments with desorption temperatures of 150 and 300°C, however,  
8 the higher pre-treatment temperature was used.

### 10 **3.5. Desorption behaviour of hydrotalcite/alumina pellets**

12 Desorption was performed in the previously described experiments by re-heating the hydrotalcite to  
13 the desorption temperature. If desorption temperature was chosen to be the same temperature as  
14 used for pre-treatment, complete desorption was observed for all the experiments (Table 2). As a  
15 temperature of 150 °C was sufficient for complete carbon dioxide desorption in the experiment with  
16 pre-treatment at 150 °C, an experiment was performed using 300 °C for pre-treatment and 150 °C for  
17 desorption. Desorption was not complete in this case, and the desorbed amount of carbon dioxide  
18 was virtually equal to the amount adsorbed and desorbed in the experiment with 150 °C as the pre-  
19 treatment and desorption temperature (Table 2). A methodical effect caused by the  
20 thermogravimetric measurement can be excluded, as temperature and buoyancy effects were  
21 checked with a non-adsorbent sample (glass beads) and proved to be negligible. Obviously high  
22 temperatures are required for complete desorption. This may show that chemisorption is involved.  
23 Note, however, that desorption in these experiments was carried out in the same gas atmosphere as  
24 the adsorption. Thus, desorption was driven merely by the change in temperature and consequent  
25 change of the adsorption equilibrium. Complete desorption was obtained for all further experiments  
26 on heating to 600 °C. Therefore, complete desorption can be achieved at high temperatures even in  
27 the atmosphere of the adsorbed gas. At lower pressure, it would certainly be possible to use lower

1 temperatures for desorption. Adsorption at lower temperatures may also be performed with  
2 nitrogen at atmospheric pressure, but some nitrogen adsorption can occur in this case.

### 3 4 **3.6. Comparison of carbon dioxide adsorption capacity upon hydrotalcite/alumina pellets**

5  
6 Fig. 11 shows the adsorbed amount of carbon dioxide on the hydrotalcite/alumina samples with  
7 variation of temperature. The results for silica gel are included in the graph for comparison.  
8 Adsorption decreases with increasing temperature, again showing virtually the same adsorption  
9 capacities for all four hydrotalcites. The overall amount of carbon dioxide adsorbed is higher than  
10 some reported studies (Choi et al., 2009). One reason is that in this study the lowest temperature at  
11 which adsorption was measured was 25 °C, whereas in the survey of Choi et al. (2009), the lowest  
12 temperature was 473 K, (200 °C). The decreasing adsorption with increasing temperature is in  
13 accordance with literature results (Othman et al., 2006), whereas a maximum adsorption was found  
14 at a temperature of 300 °C by Yong et al. (2002). It is noted that the results presented in Fig. 11 refer  
15 to dry carbon dioxide. In the presence of water vapour, adsorption capacities of hydrotalcites is  
16 expected to markedly increase.

17 There is no significant difference in the adsorption between the four different  
18 hydrotalcite/alumina samples at 150 and 300 °C. At 20 °C, Sample 6 shows a slightly higher  
19 adsorption and Sample 3 a slightly lower adsorption than the other hydrotalcites in this study.  
20 However, this small difference may arise from the experimental inaccuracy due to small differences  
21 in sample mass. From the results obtained in this study, no general trends can be seen and the  
22 adsorption seems to be independent of the hydrotalcite composition. Additionally, mixing the  
23 hydrotalcite with boehmite and calcining at 600 °C would have lead to a different structure to non-  
24 calcined hydrotalcite, incorporating particles of mixed oxide within an alumina matrix. It may be the  
25 case that some adsorption occurs over the alumina with which hydrotalcite is mixed during pellet  
26 manufacture. In that case, the composition of the hydrotalcite itself has less influence upon the

1 adsorption capacity compared with the pure non-calcined hydrotalcite, as reported in the literature  
2 (Hutson et al., 2008; Yong et al., 2002).

3 Carbon dioxide adsorption on the hydrotalcites is more than twice as high as the adsorption on  
4 silica gel under the same conditions. This shows that hydrotalcites are indeed a suitable sorbent for  
5 carbon dioxide over a wide temperature range. At 20 °C, adsorption of carbon dioxide is between  
6 2.0-2.5 mmol g<sup>-1</sup> for all the hydrotalcite samples in this study. Yong et al. (2002), reported adsorption  
7 capacities for carbon dioxide between 0.1-0.25 mmol g<sup>-1</sup> for different hydrotalcite samples at 25 °C.  
8 An adsorption capacity of approximately 0.25 mmol g<sup>-1</sup> was also found by Soares et al. (2005) at 29 °C  
9 for a hydrotalcite containing only Mg and Al as cations. In comparison, the hydrotalcites used in this  
10 study, containing different amounts of Ni and Fe, show increased carbon dioxide adsorption capacity  
11 at low temperatures. Although the adsorption capacity decreases at higher temperatures, the  
12 hydrotalcites still show higher adsorption capacity for carbon dioxide than, for example, silica gel.  
13 Amine modified functionalised SBA-12 meso-porous silicas showed adsorption capacities for carbon  
14 dioxide of up to 1.4 mmol g<sup>-1</sup> (Zelenak et al., 2008). Carbon dioxide adsorption capacities of 0.25-0.5  
15 mmol g<sup>-1</sup> at 300 °C and 0.1-0.9 mmol g<sup>-1</sup> at 200 °C (Hutson et al., 2004; Yong et al., 2002) have been  
16 reported for hydrotalcites. The results reported in this work for hydrotalcites containing Ni and Fe as  
17 cations are in the same range range, with 0.6 mmol g<sup>-1</sup> at 150 °C and 0.2 mmol g<sup>-1</sup> at 300 °C  
18 respectively.

19

### 20 **3.7. Long-term sorption behaviour**

21

22 In order to check the long-term sorption behaviour of the hydrotalcite/alumina pellet samples,  
23 several sorption experiments were performed with the same sample (Sample 3), at an elevated  
24 temperature of 150 °C, since the hydrotalcites would be exposed to higher temperatures during  
25 service in a carbon capture unit. After the first adsorption-desorption cycle the sample was allowed  
26 to cool. Another adsorption-desorption cycle was then carried out with the same sample using the

1 same experimental procedure including pre-treatment. The results are shown in Table 3. The  
2 adsorption was slightly lower for the used sample than for the fresh sample. This decrease in  
3 adsorption capacity was reproducible. It is possible that although desorption seems to be complete,  
4 some chemisorption occurs which leads to blocking of adsorption sites for subsequent adsorption  
5 cycles. However the loss in adsorption capacity of the second cycle for the calcined  
6 hydrotalcite/alumina samples was much lower than for the hydrotalcite powders, shown in Fig. 5. A  
7 slight initial decrease in adsorption capacity over several cycles has also been reported by several  
8 research groups (Hutson and Attwood, 2004; Oliveira et al., 2008; Yong et al., 2002), whereas Ebner  
9 et al. (2007) found a constant sorption behaviour over many cycles.

10

### 11 **3.8. Effect of sample morphology**

12

13 The effect of the sample morphology on the adsorption of carbon dioxide on a hydrotalcite sample  
14 was investigated. In this case, the hydrotalcite sample was used in pellet form rather than crushed to  
15 a fine powder. The result is shown in Table 3. The adsorption of carbon dioxide on the pellet was  
16 slightly lower than on the powder. More surface and possibly more pores are accessible in the  
17 powder than in the pellet, which is crucial for adsorption. Furthermore, mass transport limitations  
18 are minimised for the powder compared to the pellet. If hydrotalcites are used in a post-combustion  
19 adsorber, an optimum particle size has to be found, as a fine powder increases the pressure drop in a  
20 packed bed. In order to make a detailed assessment of the effect of particle size, both external and  
21 internal diffusion at the pellet have to be considered (Seader and Henley, 1998). For external  
22 diffusion, the mass transfer coefficient can be determined from the Sherwood number, which is  
23 correlated with Reynolds and Schmidt numbers (Ranz and Marshall, 1952):

$$24 \quad Sh = 2 + 0.6Sc^{1/3} Re^{1/2} \quad (1)$$

25 From this equation, it can be deduced that at high Reynolds numbers above 2000, where  
26  $2 \ll 0.6Sc^{1/3} Re^{1/2}$ , the mass transfer coefficient  $k_c$  is proportional to  $d_p^{-1/2}$ . Thus increasing the

1 particle size will have the effect of reducing the mass transfer coefficient and increasing external  
2 diffusion limitations. To analyze internal diffusion within the pellet, the concentration of carbon  
3 dioxide,  $C$ , as a function of the pellet radius,  $r$ , may be calculated by solving the following equation  
4 with appropriate boundary conditions:

$$5 \quad D_e \left( \frac{\partial^2 C}{\partial r^2} + \frac{2}{r} \frac{\partial C}{\partial r} \right) = \frac{\partial q}{\partial t} \quad (2)$$

6 where  $q$  is the amount adsorbed per unit volume of the porous pellet and  $D_e$  is the effective  
7 diffusivity in the pellet. The effective diffusivity is comprised of contributions from bulk and Knudsen  
8 diffusion in the gas phase and surface diffusion of adsorbed molecules upon the pore walls of the  
9 pellet. The internal pore structural parameters of porosity and tortuosity also influence the value of  
10  $D_e$  (Seader and Henley, 1998). The use of smaller particles leads to reduced internal diffusion  
11 resistance, however in a fixed bed reactor the pressure drop, calculated from the Ergun equation, is  
12 higher for smaller particles. Therefore a trade-off in selecting the optimum particle size occurs,  
13 where the particular optimum may be specific to certain adsorber designs or conditions. Typical  
14 adsorbent pellet effective diameters for gas phase applications are around 2-5 mm. Detailed designs  
15 and modelling of adsorbers for these hydrotalcites will be the subject of future investigations.

16

### 17 **3.9. Strategies for integration of adsorption processes in carbon capture and storage processes**

18

19 Application of adsorbents, amongst other possible technologies, within carbon capture and storage  
20 plants could provide a means of reducing carbon emissions from large scale point source such as  
21 power stations. Such technologies are part of a portfolio of measures to try to limit or reduce the  
22 effects of climate change (Chalmers et al., 2009). Carbon capture processes can be classified into  
23 one of three categories (Penht and Henkel, 2009):

- 24 • *Post combustion capture*, involves the separation of carbon dioxide in the flue gases from  
25 other components.

- 1 • *Pre combustion capture*, in which the fuel for the power plant is converted into carbon  
2 dioxide and hydrogen then separating the carbon dioxide from hydrogen, the latter of which  
3 is burnt in the boilers.
- 4 • *Oxyfuel*, where the combustion air is first separated into nitrogen and oxygen, such that the  
5 fuel can be burnt is pure oxygen, giving a flue gas of carbon dioxide and water vapour, from  
6 which purified carbon dioxide is easily separated.

7 Although currently absorption into liquids is favoured for pre and post combustion carbon  
8 capture, adsorption on to solid materials could avoid the handling and regeneration of potentially  
9 environmentally damaging solvents. For pre-combustion capture, where gas is at high pressure, the  
10 most suitable capture process is pressure-swing adsorption. However, in post combustion capture,  
11 the low pressure of the flue gas favours temperature swing adsorption. Therefore any adsorbent  
12 used for post combustion capture must be capable of operating at elevated temperature, for  
13 example up to 75 °C (Arenillas et al., 2005). Choi et al. (2009) reviewed the available types of  
14 adsorbents and concluded that physisorbents such as carbons and zeolites show better adsorption  
15 capacity and selectivity close to ambient temperatures. Chemisorbents such as metal oxides and  
16 hydrotalcites are able to be used up to higher temperatures (573-673 K respectively), but on the  
17 other hand can be more difficult to regenerate. Ongoing development of specialised adsorbents  
18 such as supported amines has led to higher adsorptive capacities, but their use may be limited to  
19 lower temperatures to avoid damaging the amine groups. The selection of a suitable adsorbent will  
20 depend on many factors including the adsorptive capacity, ease of regeneration, lifetime, cost and  
21 stability under process conditions.

## 22

## 23 **4. Conclusions**

## 24

25 Hydrotalcites are suitable sorbents for carbon dioxide over a wide temperature range. Although  
26 adsorption is much better at low temperatures, hydrotalcites still possess advantages over other

1 sorbents such as silica gel at high temperatures. Unlike silica gel, hydrotalcite is stable at high  
2 temperatures and still has a fairly good adsorption capacity for carbon dioxide. Prior to combination  
3 with boehmite and calcination, the hydrotalcites showed some effect of composition upon carbon  
4 dioxide uptake, with Sample 1 displaying the highest capacity and adsorption rate. However, the  
5 effect of composition upon carbon dioxide adsorption decreased upon combining with boehmite and  
6 calcining to make pellets. Ongoing testing will be used to confirm the selectivity of adsorption of  
7 carbon dioxide from mixed carbon dioxide/nitrogen gas streams, and will include humid gases under  
8 flow conditions in a fixed bed reactor. Further development of hydrotalcites could focus on  
9 intercalation of the Brucite layers with carbon dioxide accepting organic molecules such as  
10 calixarenes or attachment of basic functional groups such as amines to their surface, in order to  
11 further enhance their capability for carbon dioxide adsorption. The studies reported here with  
12 standard hydrotalcite samples measured by TGA under dry conditions will thus provide a useful  
13 benchmark for comparison with future studies modified adsorbents.

14

## 15 **Acknowledgements**

16

17 EPSRC funding is gratefully acknowledged from the “C-Cycle” project EP/010601/1 (Birmingham) and  
18 EP/E010318/1 (Sheffield).

19

## 20 **Nomenclature**

21  $a$  Unit cell dimension in the x-direction, determined by XRD (Å)

22  $c$  Unit cell dimension in the z-direction, determined by XRD (Å)

23  $C$  Concentration of solute ( $\text{kg m}^{-3}$ )

24  $d$   $d$ -spacing, the interatomic spacing, determined by XRD (Å)

25  $d_p$  Particle diameter (m)

26  $D_e$  Effective diffusivity in a pellet ( $\text{m}^2\text{s}^{-1}$ )

1	$D_i$	Diffusivity of component $i$ ( $\text{m}^2\text{s}^{-1}$ )
2	$k_c$	Mass transfer coefficient ( $\text{m s}^{-1}$ )
3	$M$	Metal ion
4	$q$	Amount adsorbed per unit volume of pellet ( $\text{kg m}^{-3}$ )
5	$r$	Pellet radius (m)
6	$Re$	Reynolds number $Re = \rho u d_p / \mu$
7	$Sc$	Schmidt number $Sc = \mu / \rho D_i$
8	$Sh$	Sherwood number $Sh = k_c d_p / D_i$
9	$t$	Time (s)
10	$u$	Fluid velocity ( $\text{m s}^{-1}$ )
11	$\mu$	Dynamic viscosity ( $\text{N s m}^{-2}$ )
12	$\theta$	Diffraction angle of XRD (degrees)
13	$\rho$	Fluid density ( $\text{kg m}^{-3}$ )
14		
15		

## 1   **References**

2

3   Arenillas, A., Smith, K.M., Drage, T.C., Snape, C.E., 2005, CO<sub>2</sub> capture using some fly ash-derived carbon  
4   materials. *Fuel*, 84: 2204 – 2210.

5   Barriga, C., Fernandez, J.M., Ulibarri, M.A., Labajos, F.M. and Rives, V., 1996, Synthesis and characterization of  
6   new hydrotalcite-like compounds containing Ni(II) and Mn (III)\_in the hydroxide layers and of their calcination,  
7   *J Solid State Chem*, 124: 205 – 213.

8   Bhattacharyya, A., Chang, V.W. and Schumacher, D.J., 1998, CO<sub>2</sub> reforming of methane to syngas I: evaluation  
9   of hydrotalcite clay-derived catalysts, *Appl Clay Sci* 12:317 – 328.

10   Bhattacharyya, A. and Hall, D.B., New triborate-pillared hydrotalcites, 1992, *Inorganic Chem*, 31, 3869 – 3870.

11   Carja, G., Nakamura, R., Aida, T, Niiyama, H., 2001, Textural properties of layered double hydroxides: effect of  
12   magnesium substitution by copper or iron, *Micropor Mesopor Mat*, 47: 275 – 284.

13   Carpani, I., Berrettoni, M., Ballarin, B., Giorgetti, M., Scavetta, E., Tonelli, D., 2004, Study on the intercalation of  
14   hexacyanoferrate(II) in a Ni, Al based hydrotalcite, *Solid State Ionics*, 168: 167-175.

15   Carrado, K.A., Csencsits, R., Thiyagaragjan, P, Seifert, S., Macha, S.M., Harwood, J.S., 2002, Crystallization and  
16   textural porosity of synthetic clay minerals, *Mater Chem*, 12: 3228 – 3237.

17   Cavani, F., Trifiro, F. and Vaccari, A., 1991, Hydrotalcite-type anionic clays: preparation, properties and  
18   applications, *Catal Today* 11: 173 – 301.

19   Chalmers, H., Jakeman, N., Pearson, P., Gibbins, J., 2009, Carbon capture and storage deployment in the UK:  
20   what next after the UK government's competition? *Proc. IMechE* 223 Part A:305 – 319.

21   Chmielarz, L., Kustrowski, P., Rafalska-Lasocha, A., Majda, D., Dziembaj, R., 2002, Catalytic activity of Co-Mg-Al,  
22   Cu-Mg-Al and Cu-Co-Mg-Al mixed oxides derived from hydrotalcites in SCR of NO with ammonia. *Appl Catal B*,  
23   35: 195 - 210.

24   Choi, S., Drese, J.H. and Jones, C.W., 2009, Adsorbent materials for carbon dioxide capture from large  
25   anthropogenic point sources. *Chem Sus Chem*, 2: 796 – 854.

26   Clause, O., Goncalves Coelho, M., Gazzano, M.,Matteuzzi, D., Trifirò, F. and Vaccari, A., 1992, Synthesis and  
27   thermal reactivity of nickel-containing anionic clays, *Appl Clay Sci*, 8: 169 – 186.,

1 Climent, M.J., Corma, A., Iborra, S., Epping, K., and Velty, A., 2004, Increasing the basicity and catalytic activity  
2 of hydrotalcites by different synthesis procedures, *J Catal*, 225: 316 – 326.

3 Costantino, U., Marmottini, F., Nocchetti, M., Vivani, R., 1998, New synthetic routes to hydrotalcite-like  
4 compounds – Characterisation and properties of the obtained materials, *Europ J Inorg Chem*: 1439-1446.

5 Courson, C., Makaga, E., Petit, C., Kiennemann, A., 2000, Development of Ni catalysts for gas production from  
6 biomass gasification. Reactivity in steam- and dry-reforming, *Catal Today*, 63: 427 – 437.

7 Ebner, A.D., Reynolds, S.P. and Ritter, J.A., 2007, Nonequilibrium kinetic model that describes the reversible  
8 adsorption and desorption behavior of CO<sub>2</sub> in a K-promoted hydrotalcite-like compound, *Ind Eng Chem Res*,  
9 46, 1737 – 1744.

10 Huang, H.Y., Yang, R.T., Chinn, D., Munson, C.L., 2003, Amine-grafted MCM-48 and silica xerogel as superior  
11 sorbents for acidic gas removal, *Ind Eng Chem Res*, 42: 2427 – 2433.

12 Hutson, N.D. and Attwood, B.C., 2008, High temperature adsorption of CO<sub>2</sub> on various hydrotalcite-like  
13 compounds, *Adsorption*, 14: 781 – 789.

14 Hutson, N.D., Speakman, S.A. and Payzant, E.A., 2004, Structural effects on the high temperature adsorption of  
15 CO<sub>2</sub> on a synthetic hydrotalcite. *Chem Mater*, 16: 4135 – 4143.

16 Kloprogge, J.T., Hickey, L., Frost, R.L., 2005, The effect of varying synthesis conditions on zinc chromium  
17 hydrotalcite: a spectroscopic study, *Mater Chem Phys*, 89: 99 – 109.

18 Intergovernmental Panel on Climate Change, IPCC Fourth Assessment Report (AR4), 2007, <http://www.ipcc.ch/>.

19 Li, C., and Chen, Y.W., 1995, Temperature-programmed-reduction studies of nickel oxide/alumina catalysts:  
20 effects of the preparation method, *Thermochim Acta*, 256, 457 – 465.

21 Lwin, Y. and Abdullah, F., 2009, High temperature adsorption of carbon dioxide on Cu-Al hydrotalcite-derived  
22 mixed oxides: kinetics and equilibria by thermogravimetry, *Journal of Thermal Analysis and Calorimetry*, 97:  
23 885 – 889.

24 Majchrzak-Kuceba, I. and Nowak, W., 2005, A thermogravimetric study of the adsorption of CO<sub>2</sub> on zeolites  
25 synthesized from fly ash, *Thermochimica Acta*, 437: 67 – 74.

26 Malet, P. and Caballero, A., 1988, The selection of experimental conditions in temperature-programmed  
27 reduction experiments, *J Chem Soc Faraday Trans I*, 84: 2369-2375.

28 Montoya, J.A., Romero-Pascual, E., Gimón, C., Del Angel, P., Monzon, A., 2000, Methan reforming with CO<sub>2</sub>  
29 over Ni/ZrO<sub>2</sub>-CeO<sub>2</sub> catalysts prepared by sol-gel, *Catal Today*, 63: 71-85.

1 Mosqueda, H.A., Vaquez, C., Bosch, P and Pfeiffer, H., 2006, Chemical sorption of carbon dioxide (CO<sub>2</sub>) on  
2 lithium oxide (Li<sub>2</sub>O), *Chem Mater* 18: 2307 – 2310.

3 Ohishi, Y., Kawabata, T., Shishido, T., Takaki, K., Zhang, Q.H., Wang, Y., Nomura, K., and Takehira, 2005, Mg-Fe-  
4 Al mixed oxides with mesoporous properties prepared from hydrotalcite as precursors: Catalytic behavior in  
5 ethylbenzene dehydrogenation, *Appl Catal A*, 288, 220 – 231.

6 Olafsen, A., Slagern, A., Dahl, I.M., Olsbye, U., Schuurman, Y., Mirodatos, C., 2005, Mechanistic features for  
7 propane reforming by carbon dioxide over a Ni/Mg(Al)O hydrotalcite-derived catalyst, *J Catal*, 229: 163 – 175.

8 Oliveira, E.L.G., Grande, C.A. and Rodrigues, A.E., 2008, CO<sub>2</sub> sorption on hydrotalcite and alkali-modified (K and  
9 Cs) hydrotalcites at high temperatures, *Sep Purific Technol*, 62: 137 – 147.

10 Othman, M.R., Rasid, N.M., Fernando, W.J.N., 2006, Mg-Al hydrotalcite coating on zeolites for improved carbon  
11 dioxide adsorption, *Chem Eng Sci*, 61: 1555-1560.

12 Parmaliana, A., Arena, F., Frusteri, G., Giordano, N., 1990, Temperature-programmed reduction study of NiO-  
13 MgO Interactions in magnesia-supported Ni catalysts and NiO-MgO physical mixture, *J Chem Soc Faraday T*, 86:  
14 2663-2669.

15 Pehnt, M. and Henkel, J., 2009, Life cycle assessment of carbon dioxide capture and storage from lignite power  
16 plants, *International Journal of Greenhouse Gas Control*, 3: 49 – 66.

17 Perez-Lopez O.W., Senger, A., Marcilio, N.R., Lansarin, M.A., 2006, Effect of composition and thermal  
18 pretreatment on properties of NiMgAl catalysts for CO<sub>2</sub> reforming of methane, *Appl Catal A* , 303:234-244.

19 Radosz, M., Hu, X.D., Krutkramelis, K., Shen, Y.Q., 2008, Flue-gas carbon capture on carbonaceous sorbents:  
20 Toward a low cost multifunction carbon filter for “green” energy producers, *Ind Eng Chem Res*, 47: 3783 –  
21 3794.

22 Ranz, W.E. and Marshall, W.R., 1952, Evaporation from drops 2, *Chem Eng Prog* 48: 173 – 180.

23 Roesch, A., Reddy, E.P., Smirniotis, P.G., 2005, Parametric study of Cs/CaO sorbents with respect to simulated  
24 flue gas at high temperatures, *Ind Eng Chem Res*, 44: 6485 – 6490.

25 Seader, J.D. and Henley, E.J., 1998, *Separation Process Principles*, Chapter 15, (John Wiley and Sons, New York,  
26 USA), pp 812-818.

27 Sing, K.S.W., Everett, D.H., Haul, R.A.W., Moscou, L., Pierotti, R.A., Rouquerol, J., Siemieniewska, T., 1985,  
28 Reporting physisorption data for gas solid systems with special reference to the determination of surface area  
29 and porosity (recommendations 1984), *Pure Appl Chem*, 57: 603 – 619.

1 Soares, J.L., Casarin, G.L., Jose, H.J., Moreira, R.D.F.P.M., 2005, Experimental and theoretical analysis for the  
2 CO<sub>2</sub> adsorption on hydrotalcite, *Adsorption*, 11: 237 – 241.

3 Takehira, K., Shishido, T., Wang, P., Kosaka, T. and Takaki, K., 2003, Steam reforming of CH<sub>4</sub> over supported Ni  
4 catalysts prepared from a Mg-Al hydrotalcite-like anionic clay. *Phys Chem Chem Phys*, 5: 3801 – 3810.

5 Tamura, H., Chiba, J., Ito, M., Takeda, T., Kikkawa, S., 2004, Synthesis and characterization of hydrotalcite-ATP  
6 intercalates, *Solid State Ionics*, 172, 607 – 609.

7 Tichit, D., Medina, F., Coq, B. and Dutartre, R., 1997, Activation under oxidizing and reducing atmosphere of Ni-  
8 containing layered double hydroxides, *Appl Catal A*, 159: 241 – 258.

9 Tsyganok, A.I., Tsunoda, T., Hamakawa, S., Suzuki, K., Takehira, K., Hayakawa, T., 2003, Dry reforming of  
10 methane over catalysts derived from nickel-containing Mg-Al layered double hydroxides, *J Catal*, 213: 191 –  
11 203.

12 Unnikrishnan, R. and Narayanan, S., 1999, Metal containing layered double hydroxides as efficient catalyst  
13 precursors for the selective conversion of acetone, *J Mol Catal A*, 144: 173 – 179.

14 Walspurger, S., Boels, L., Cobden, P.D., Elzinga, G.D. Haije, W.G., van den Brink, R.W., 2008, The crucial role of  
15 the K<sup>+</sup>-aluminium oxide interaction in K<sup>+</sup>-promoted alumin- and hydrotalcite-based materials for CO<sub>2</sub> sorption  
16 at high temperatures, *Chem Sus Chem*, 1: 643 – 650.

17 Wang, X.P., Yu, J.J., Cheng, J., Hao, Z.P. and Xu, Z.P., 2008, High-temperature adsorption of carbon dioxide on  
18 mixed oxides derived from hydrotalcite-like compounds, *Environmental Science and Technology*, 42:614 – 618.

19 Wang, Y. and Levan, M.D., 2009, Adsorption equilibrium of carbon dioxide and water vapor on zeolites 5A and  
20 13X and silica gel: pure components, *J Chem Eng Data*, 54: 2839 – 2844.

21 Yong, Z., Mata, V. and Rodrigues, A.E., 2002, Adsorption of carbon dioxide at high temperature – a review, *Sep*  
22 *Purif Technol*, 26: 195 – 205.

23 Yong, Z. and Rodrigues A.E., 2002, Hydrotalcite-like compounds as adsorbents for carbon dioxide, *Energy*  
24 *Conversion and Management*, 43: 1865 – 1876.

25 Yu, Z. Chen, D., Ronning, M., Torbjorn, V., Ochoa-Fernández, E., Holmen, A., 2008, Large-scale synthesis of  
26 carbon nanofibers on Ni-Fe-Al hydrotalcite derived catalysts. I. Preparation and characterization of the Ni-Fe-  
27 Al hydrotalcites and their derived catalysts, *Appl Catal A*, 338: 136 – 146.

- 1 Zelenak, V., Halamova, D., Gaberova, L., Bloch, E., Llewellyn, P, 2008, Amine-modified SBA-12 mesoporous silica
- 2 for carbon dioxide capture: Effect of amine basicity on sorption properties, Micropor and Mesopor Mat, 116:
- 3 358 – 364.
- 4
- 5

1 **List of Figure and Table Captions**

2

3 Fig. 1. A BET adsorption isotherm for the mixed oxide prepared by calcining NiMgAl (Sample 1) hydrotalcite in  
4 static air at 600°C for 6 hours

5 Fig. 2. Powder XRD trace of the synthesised NiMgAl (Sample 1) hydrotalcite

6 Fig. 3. Powder XRD trace of the mixed oxide prepared by the calcination of Sample 1

7 Fig. 4. TPR traces for the NiMgAl (Sample 1) hydrotalcite derived mixed oxide

8 Fig. 5. Comparison of adsorption capacity of hydrotalcites, mixed oxides and boehmite powders, measured by  
9 TGA at 25 °C.

10 Fig. 6. Specific rate of adsorption for hydrotalcites, mixed oxides and boehmite powders, measured by TGA at  
11 25 °C.

12 Fig. 7. Thermogravimetric analysis of Sample 3 in carbon dioxide and nitrogen on heating from 30 to 600 °C at  
13 a heating rate of 10 °C min<sup>-1</sup>.

14 Fig. 8. Thermogravimetric analysis of hydrotalcite Samples 3 - 6 in carbon dioxide on heating from 30 to 600 °C  
15 at a heating rate of 10 °C min<sup>-1</sup>.

16 Fig. 9. Thermogravimetric analysis of silica gel in carbon dioxide on heating from 30 to 600 °C at a heating rate  
17 of 10 °C min<sup>-1</sup>.

18 Fig. 10. Thermogravimetric analysis of Sample 3 in carbon dioxide on heating from 30 to 600 °C at a heating  
19 rate of 10 °C min<sup>-1</sup> with two subsequent cooling and re-heating cycles.

20 Fig. 11. Adsorption of dry carbon dioxide on hydrotalcites (Samples 3 -6) and silica gel as a function of  
21 temperature at atmospheric pressure and 100% CO<sub>2</sub> atmosphere.

22

23 Table 1. A comparison of the surface area and textural properties of various hydrotalcite derived mixed oxides.

24 Samples 1 and 2 were used in non-calcined form. Samples 3 – 6 were calcined at 600 °C in air.

25 Table 2. Adsorption and desorption of carbon dioxide at different pre-treatment and desorption temperatures;  
26 Sample 3 was calcined at 600 °C

27 Table 3. Adsorption of carbon dioxide on Sample 3 at 150 °C under different sample conditions

Figure 1  
[Click here to download high resolution image](#)

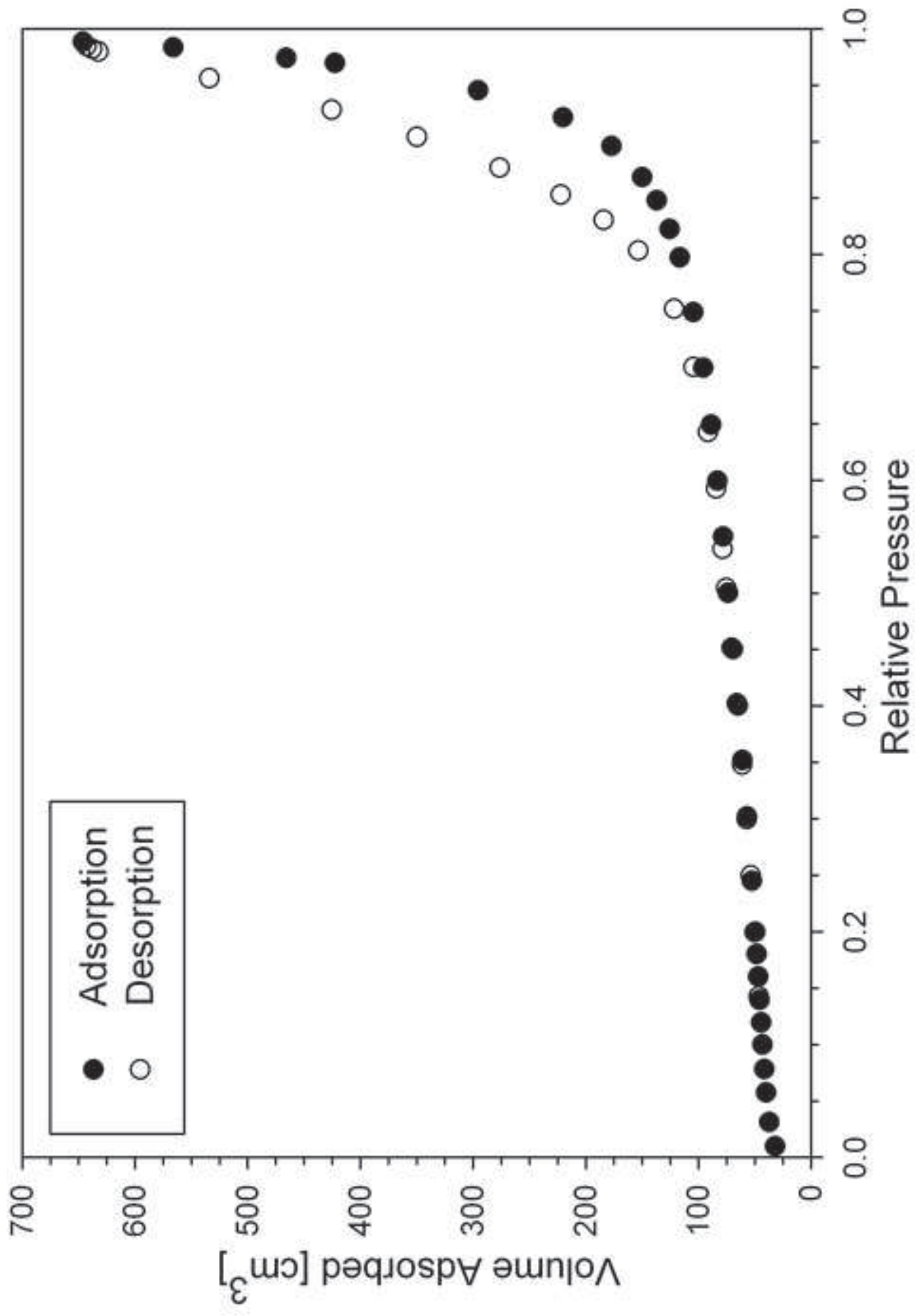


Figure 2  
[Click here to download high resolution image](#)

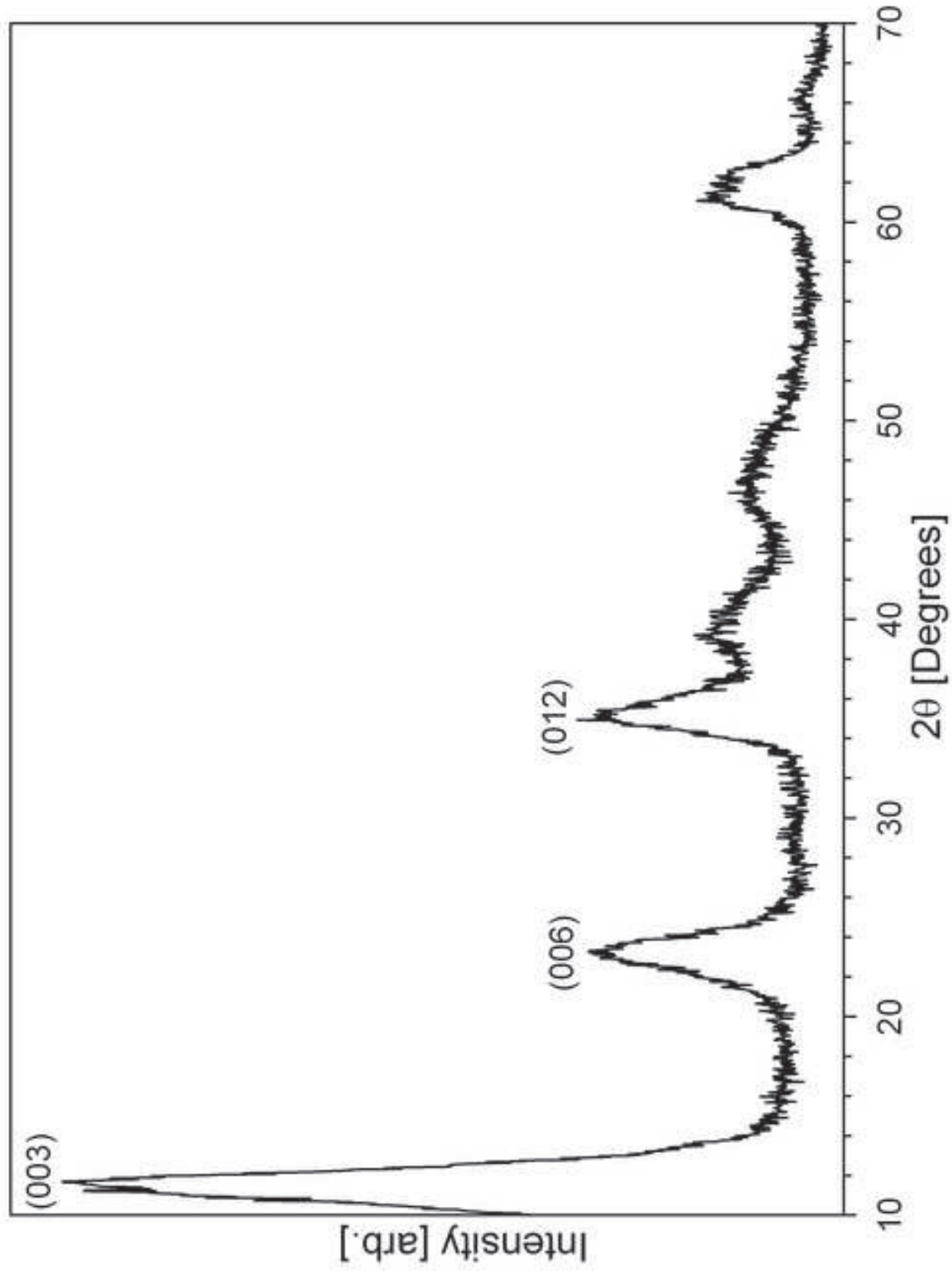


Figure 3  
[Click here to download high resolution image](#)

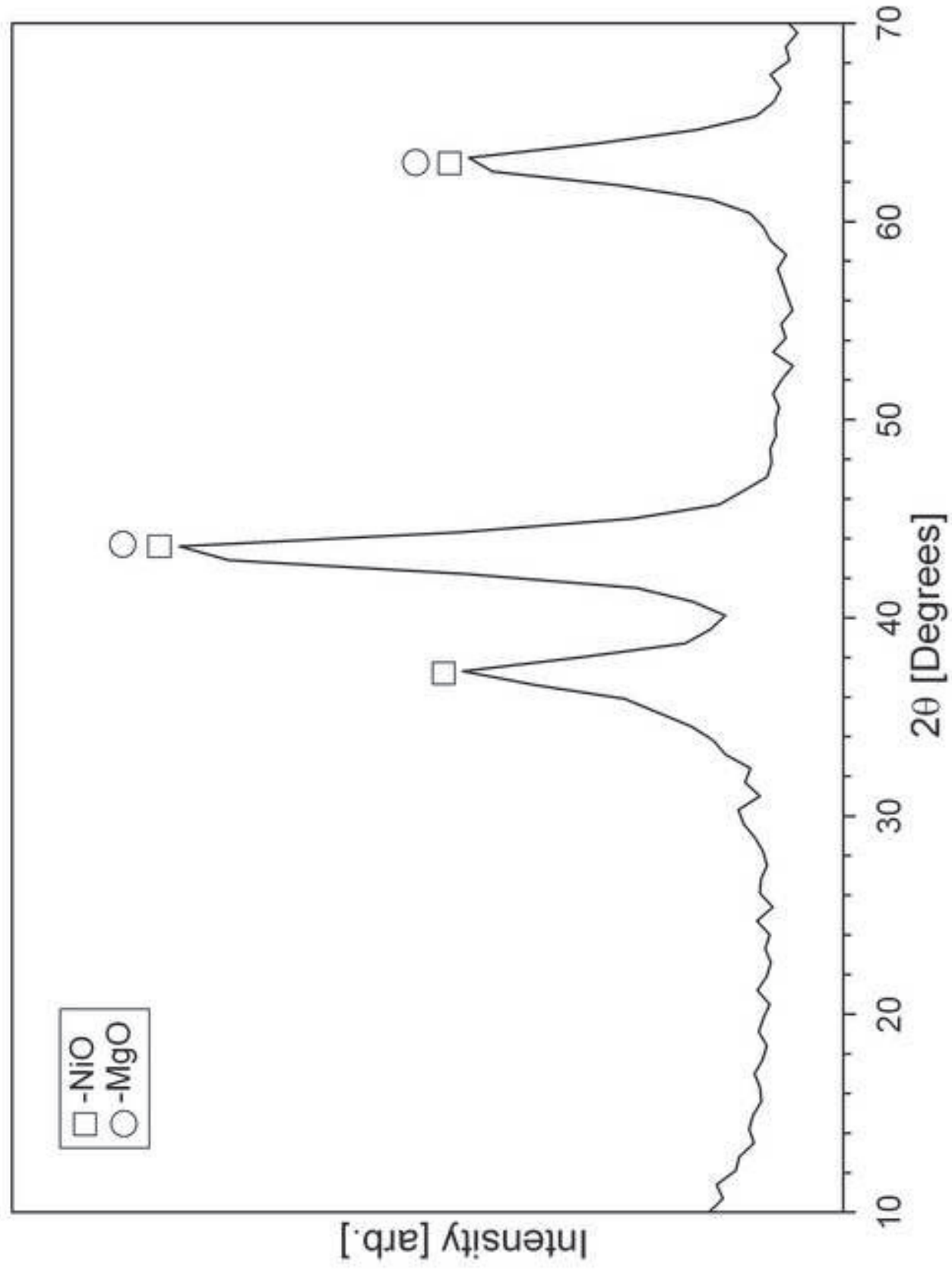


Figure 4  
Click here to download high resolution image

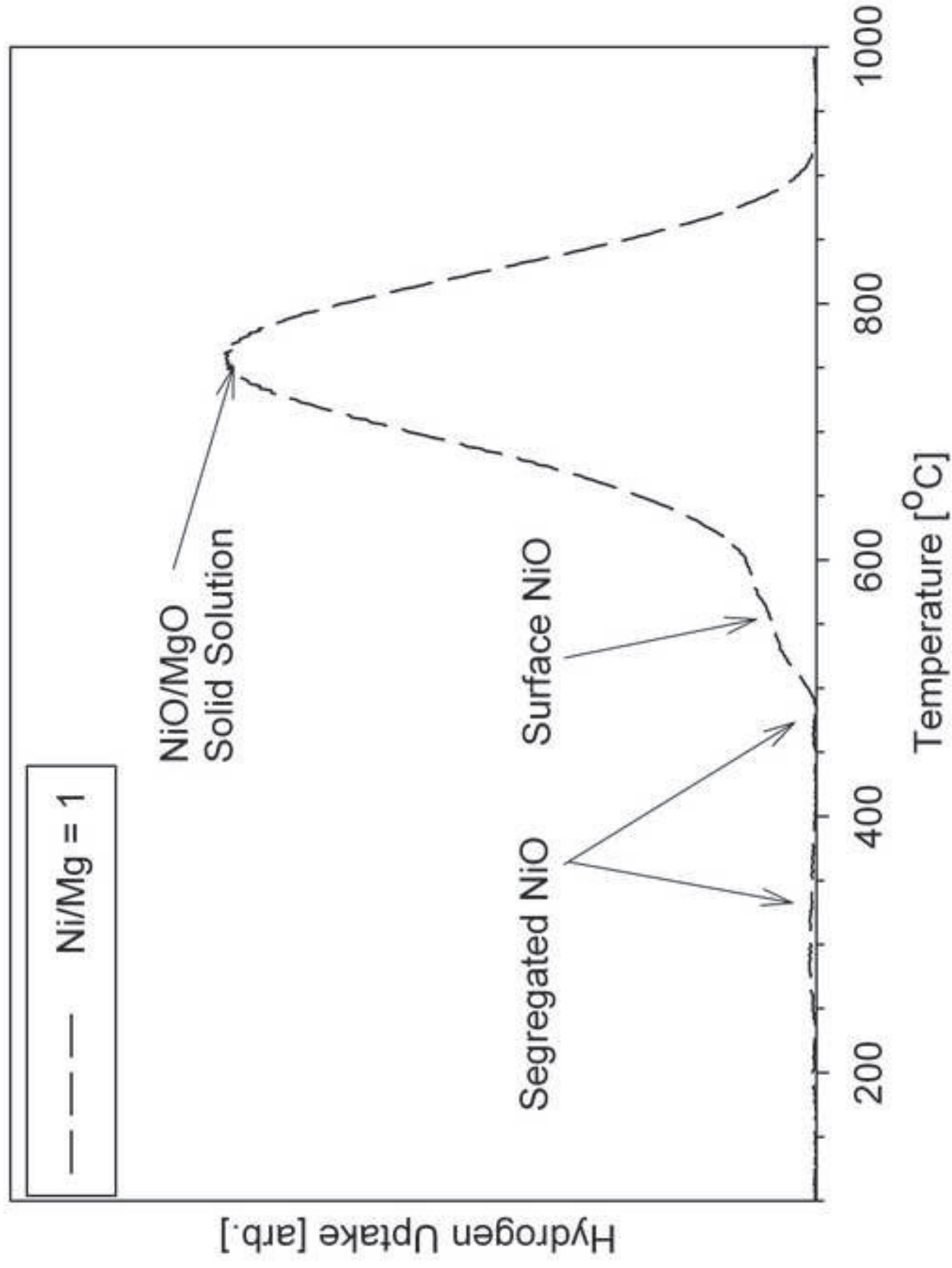


Figure 5  
[Click here to download high resolution image](#)

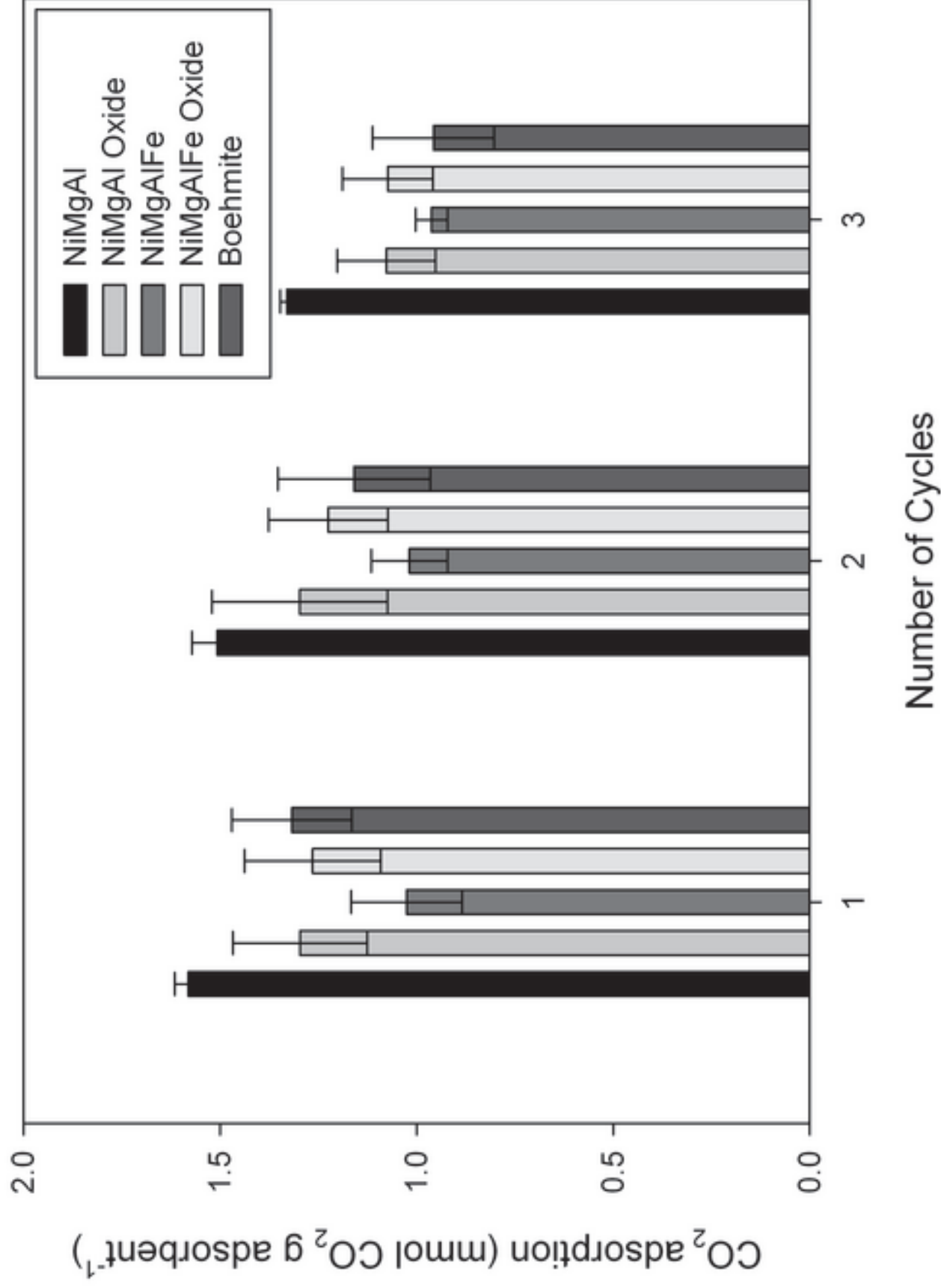


Figure 6  
[Click here to download high resolution image](#)

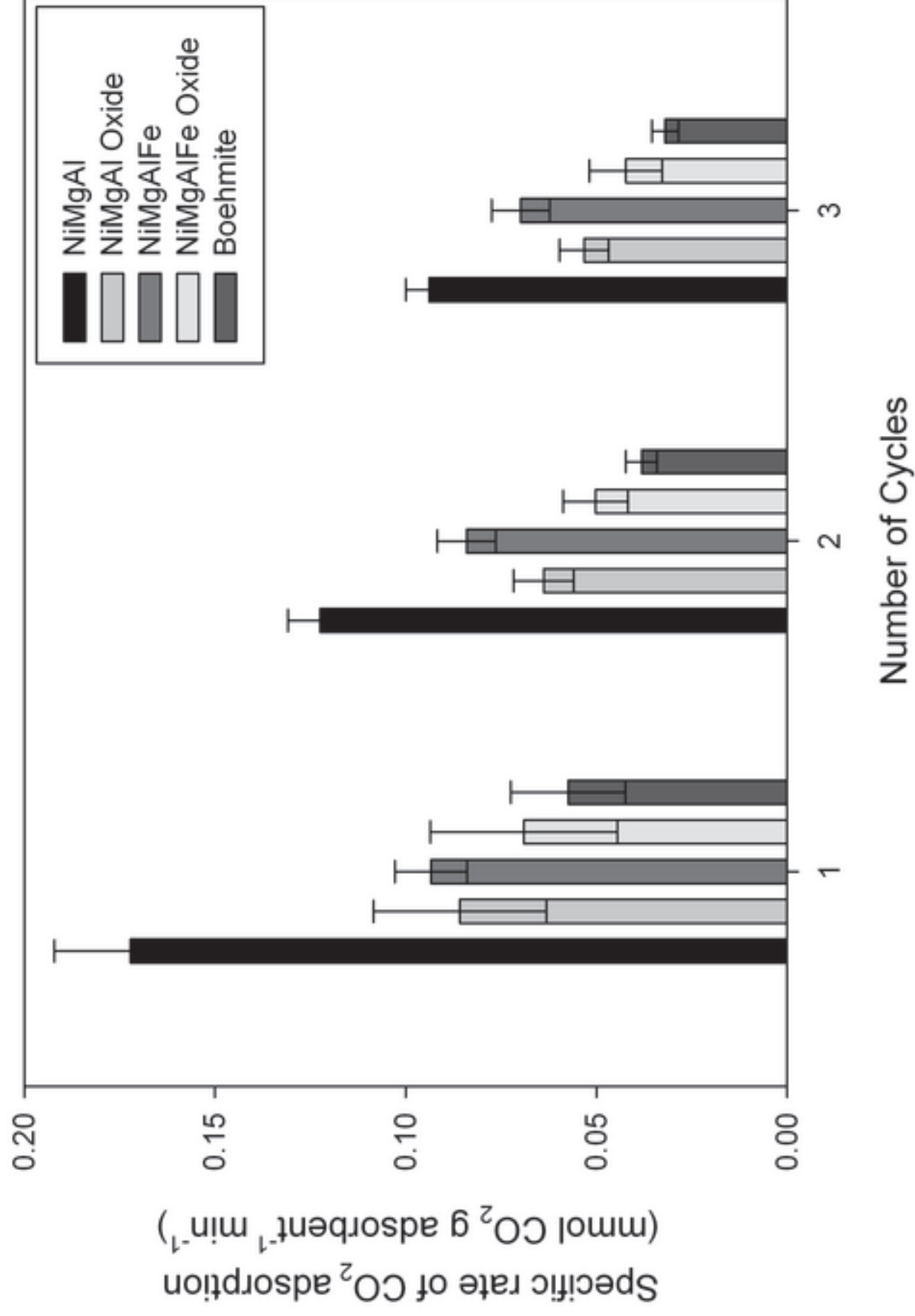


Figure 7  
[Click here to download high resolution image](#)

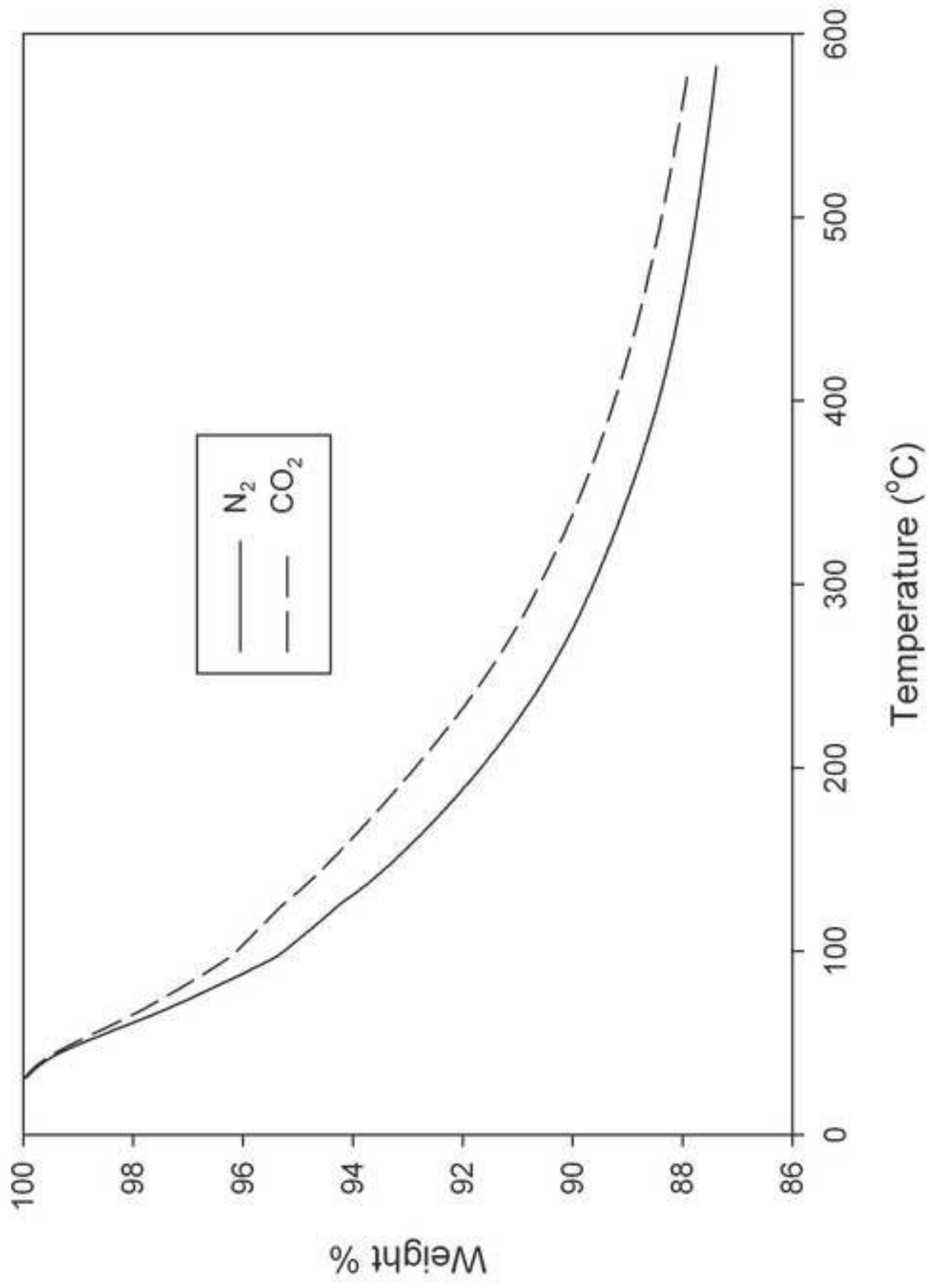


Figure 8  
[Click here to download high resolution image](#)

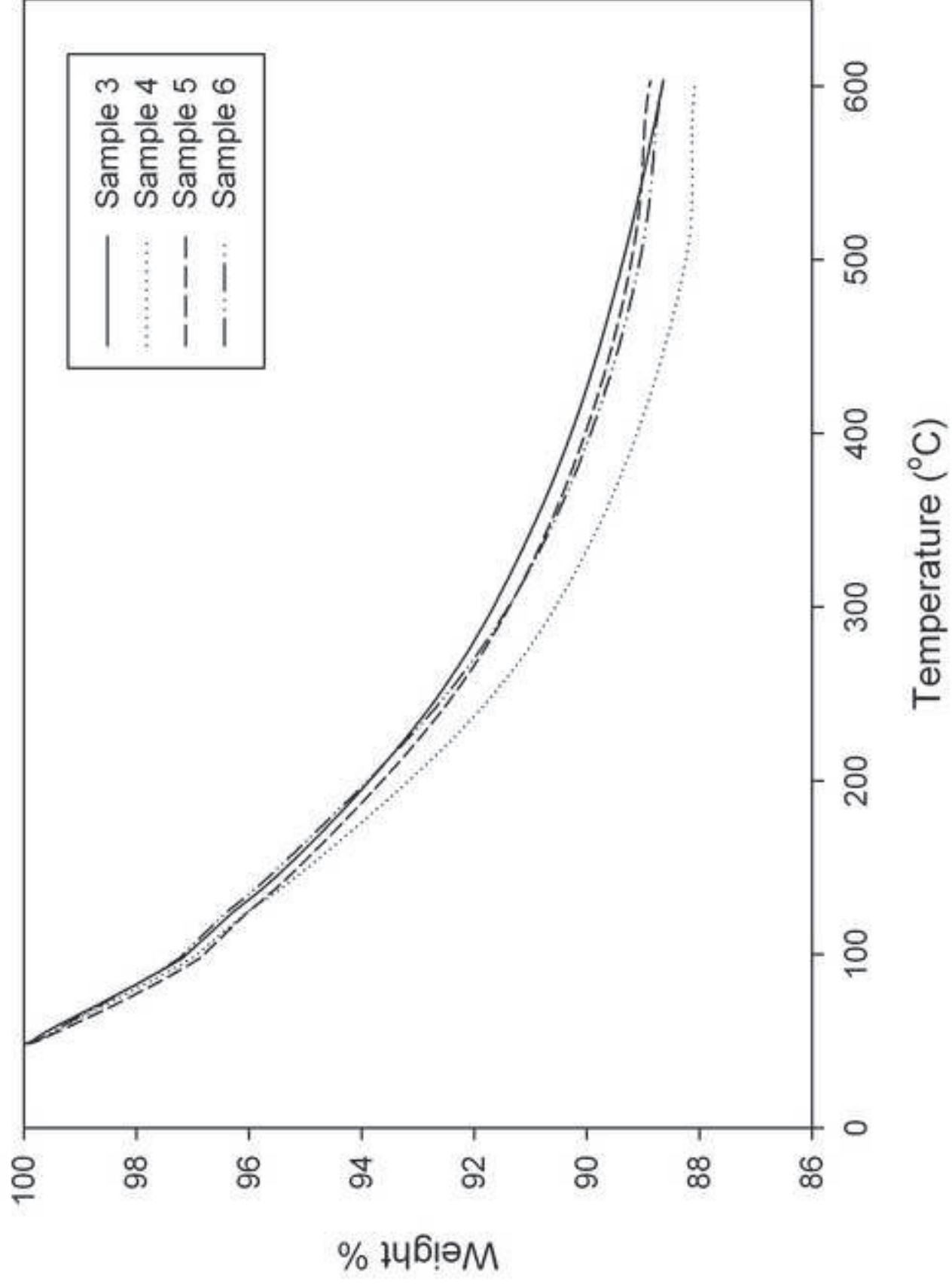


Figure 9  
[Click here to download high resolution image](#)

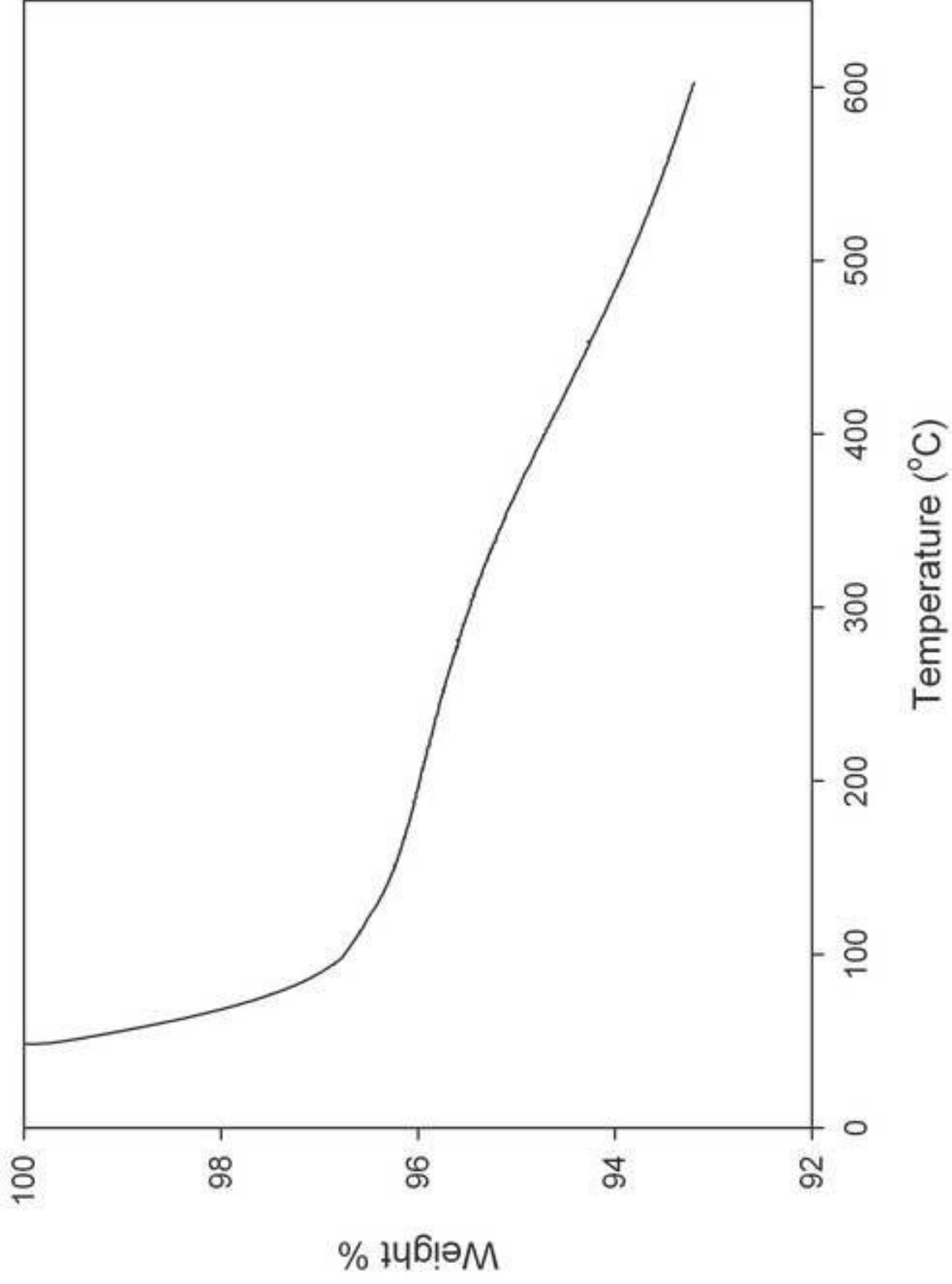


Figure 10  
[Click here to download high resolution image](#)

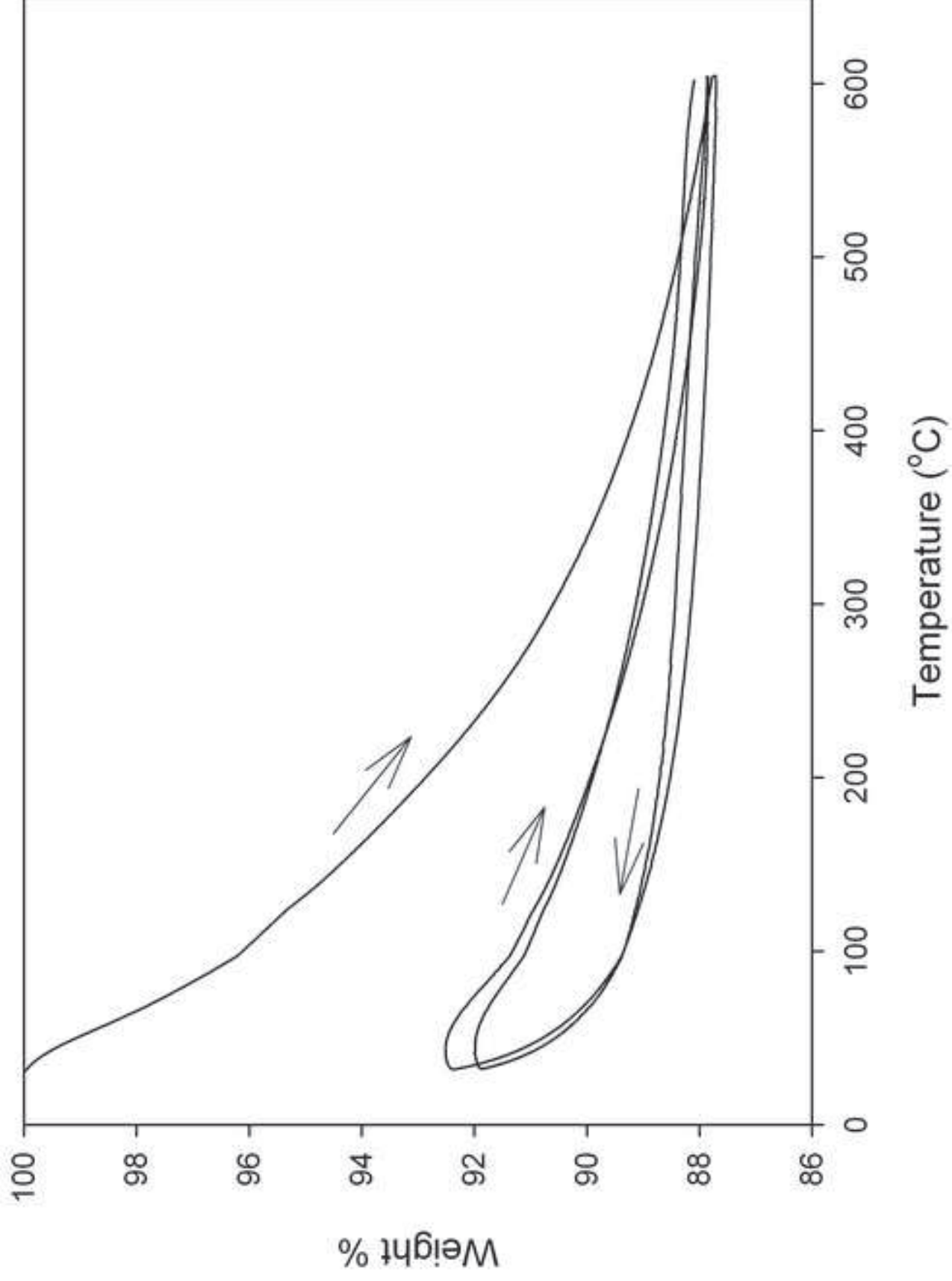
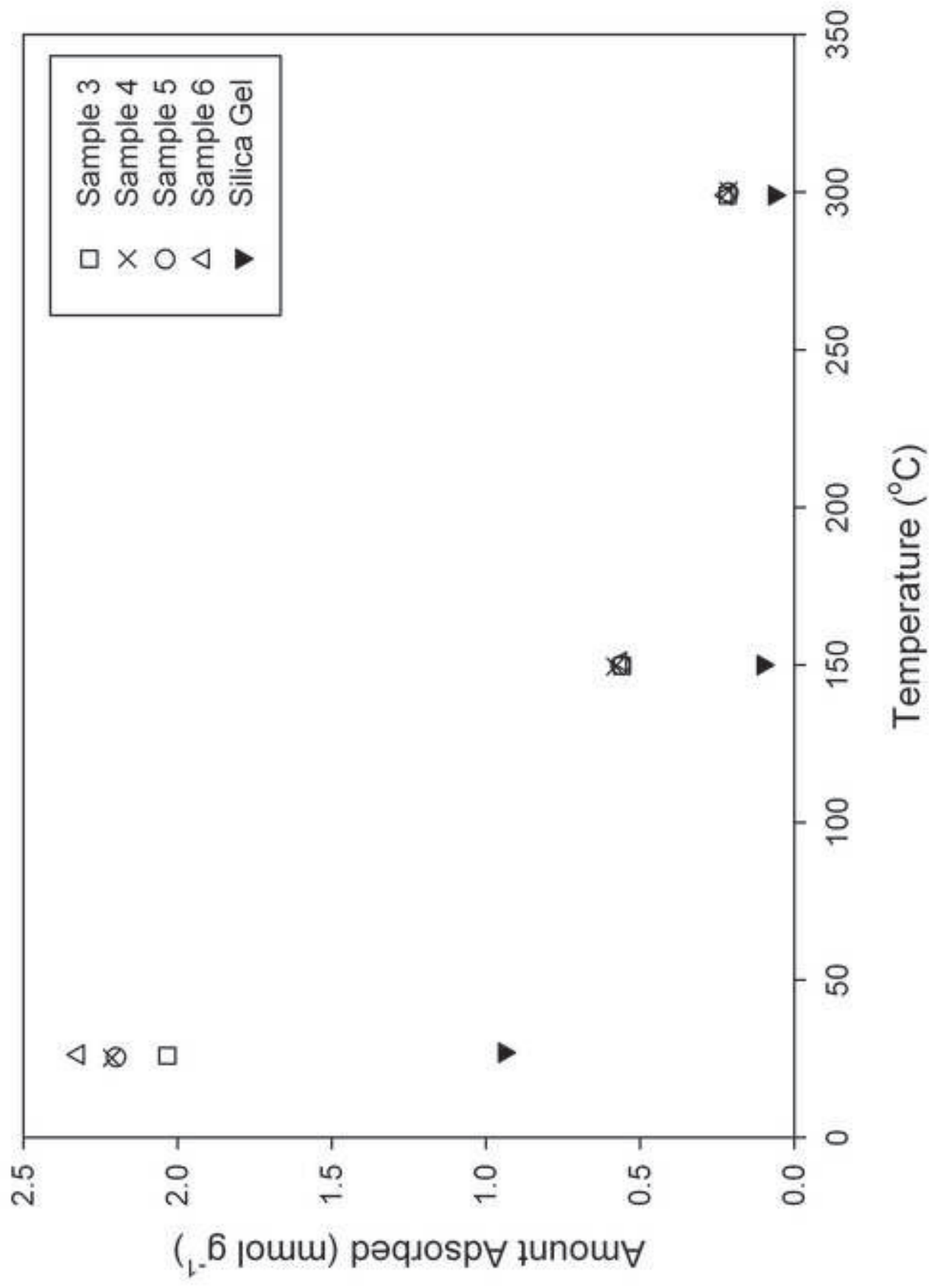


Figure 11  
[Click here to download high resolution image](#)



**Table**

Table 1. A comparison of the surface area and textural properties of various hydrotalcite derived mixed oxides. The surface areas reported for Sample 1 and 2 refer to the non-calcined form. Sample 3 – 6 were calcined at 600 °C in air.

Sample	Surface area m <sup>2</sup> g <sup>-1</sup>
<b>Sample 1</b> Ni <sup>2+</sup> /Mg <sup>2+</sup> /Al <sup>3+</sup> (0.334:0.333:0.333) powder	186.7
<b>Sample 2</b> Ni <sup>2+</sup> /Mg <sup>2+</sup> /Al <sup>3+</sup> /Fe <sup>3+</sup> (0.334:0.333:0.233:0.1) powder	156.4
Boehmite powder	265.7 ± 7.8
<b>Sample 3</b> Ni <sup>2+</sup> /Mg <sup>2+</sup> /Al <sup>3+</sup> (0.334:0.333:0.333) (50% Htlc:50% boehmite pellet)	234 ± 0.3
<b>Sample 4</b> Ni <sup>2+</sup> /Mg <sup>2+</sup> /Al <sup>3+</sup> (0.334:0.333:0.333) (70% Htlc:30% boehmite pellet)	200 ± 0.3
<b>Sample 5</b> Ni <sup>2+</sup> /Mg <sup>2+</sup> /Al <sup>3+</sup> /Fe <sup>3+</sup> (0.334:0.333:0.233:0.1) (50% Htlc:50% boehmite pellet)	218 ± 0.4
<b>Sample 6</b> Ni <sup>2+</sup> /Mg <sup>2+</sup> /Al <sup>3+</sup> /Fe <sup>3+</sup> (0.334:0.333:0.233:0.1) (70% Htlc:30% boehmite pellet)	206 ± 1.3

Table 2. Adsorption and desorption of carbon dioxide at different pre-treatment and desorption temperatures; Sample 3 was calcined at 600 °C.

<b>Substance</b>	<b>Pre-treatment</b>	<b>CO<sub>2</sub> adsorption at 20 °C in mmol g<sup>-1</sup></b>	<b>Desorption temperature</b>	<b>Desorption</b>
Sample 3	150 °C (60 min)	1.0	150 °C	Complete
Sample 3	300 °C (60 min)	1.5	300 °C	Complete
Sample 3	600 °C (10 min)	2.0	600 °C	Complete
Sample 3	300 °C (60 min)	1.5	150 °C	1.1 mmol g <sup>-1</sup> desorbed
Silica gel	150 °C (60 min)	0.9	150 °C	Complete
Silica gel	600 °C (10 min)	0.5	600 °C	Complete; some decomposition

Table 3: Adsorption of carbon dioxide on Sample 3 at 150 °C under different sample conditions.

<b>Substance</b>	<b>Form</b>	<b>Sorption cycle</b>	<b>CO<sub>2</sub> adsorption in mmol g<sup>-1</sup></b>
Sample 3	Powder	First	0.56
Sample 3	Powder	Second	0.52
Sample 3	Pellet	First	0.52